Applied Surface Science Advances 13 (2023) 100361

Contents lists available at ScienceDirect

Applied Surface Science Advances

journal homepage: www.sciencedirect.com/journal/applied-surface-science-advances

Porous thin films with hierarchical structures formed by self-assembly of zwitterionic comb copolymers

Papatya Kaner, Ilin Sadeghi, Ayse Asatekin *

Department of Chemical and Biological Engineering, Tufts University, Medford, MA 02155, USA

ARTICLE INFO

Keywords:
Hierarchical
Zwitterionic comb copolymer
Self-assembly
Porous thin film
Ionic strength responsive

ABSTRACT

Zwitterions exhibit high dipole moments and strong intra- and inter-molecular interactions. As a result, amphiphilic copolymers with zwitterionic repeat units easily self-assemble. Here, we explore the wide range of self-assembled morphologies formed by zwitterionic comb-shaped copolymers (ZCCs) comprising a hydrophobic backbone and zwitterionic side-chains. We study the effect of polymer structure, architecture, and film preparation method on self-assembled morphology. We synthesized ZCCs with varying zwitterionic side chain density and length, and applied each ZCC as a thin film on glass substrates using different methods. We compared the morphology of these films with ZCCs films coated on a porous substrate by non-solvent induced phase separation, creating mechanically supported thin films (MSTFs) and comparing them with films on non-porous substrates. The porous support led to distinct changes in film morphology, creating hierarchical features including ~17 nm spherical micelles along with larger nanopores (~85 nm). This feature size could be tuned using a zwitterionic homopolymer additive. MSTFs exhibited significant changes in water permeance and morphology upon exposure to saline solutions, known to stimulate expansion of the zwitterionic side-chains. These results demonstrate the wide range of morphologies accessible by this comb copolymer family and document the significant effect of a porous support on the film formation process.

1. Introduction

Polymer self-assembly is a powerful approach for creating nano-scale structures using scalable, bottom-up methods. Self-assembling copolymers can create highly regular structures with monodisperse size [1–3], hierarchical structures [4–6], porous materials [7–9], micelles [10], vesicles [10], and other interesting morphologies [11]. Self-assembly in free-standing or supported thin films is of particular interest for many applications including the manufacture of filtration membranes [5,9,11-19], patterning materials for information technology [20,21], solar cells [21], and others [22–24]. The self-assembled domain morphology and size is controlled by the polymer structure, polymer architecture, and processing parameters such as the use of additives, exposure to solvents, mechanical stresses, magnetic fields, etc. [8,21,23,25-27]

The wide variety of morphologies accessible through polymer self-assembly includes hierarchical structures characterized by features at multiple length scales [28]. Hierarchical structures are ubiquitous in nature, and serve crucial roles in many phenomena including super-hydrophobicity [29,30]. self-cleaning [31], adhesion [32,33], bone toughness [34], and catalysis [35]. Many researchers have mimicked these phenomena, utilizing hierarchical structures for separation membranes with improved capabilities, multi-functional materials, catalytic systems, microfluidic devices [36], and many other applications [35]. Generating such hierarchical structures by polymer self-assembly is of great interest, because this bottom-up approach easily leverages and plugs into large-scale manufacturing processes [37]. This enables new technologies to be scaled up more easily and reliably.

Abbreviations: BCP, Block copolymer; LCM, Large compound micelle; LCV, Large compound vesicle; PEO, Poly(ethylene oxide); ZCC, Zwitterionic comb copolymer; PTFEMA, Poly(2,2,2-trifluoroethyl methacrylate); SBMA, Sulfobetaine methacrylate; SB2VP, Sulfobetaine 2-vinyl pyridine; NIPS, Non-solvent indiced phase separation; MSTF, Mechanically supported thin film; CEM, 2-chloroethyl methacrylate; AIBN, Azobisisobutyronitrile; MEHQ, monomethyl ether of hydroquinone; PMDETA, N,N,N',N'',N''-pentamethyldiethylenetriamine; TFE, Trifluoroethanol; IPA, Isopropyl alcohol; THF, Tetrahydrofuran; AFM, Atomic force microscopy; NMR, Nuclear magnetic resonance; SEM, Scanning electron microscopy; PBS, Phosphate buffered saline; ARGET-ATRP, Activators ReGenerated by Electron Transfer Atom Transfer Radical Polymerization; GPC, Gel permeation chromatography; PDI, Polydispersity index; Tg, Glass transition temperature.

* Corresponding author.
E-mail address: Ayse.Asatekin@tufts.edu (A. Asatekin).

https://doi.org/10.1016/j.apsadv.2022.100361
Received 26 May 2022; Received in revised form 9 December 2022; Accepted 22 December 2022

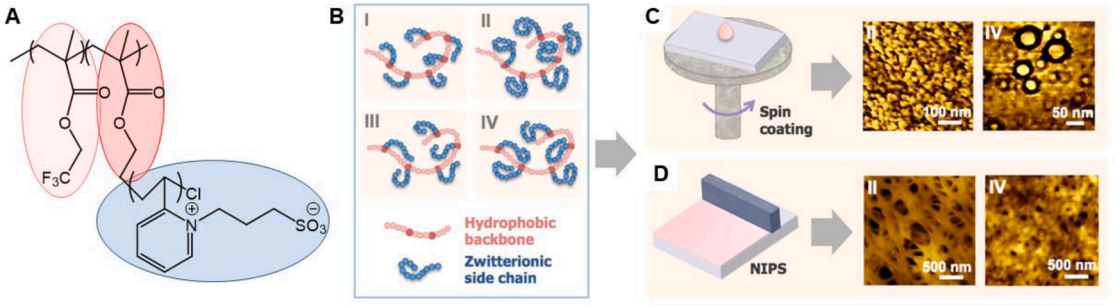

Fig. 1. ZCCs applied as a thin film on glass substrate by spin coating or non-solvent induced phase separation (NIPS).

To date, most studies on polymer self-assembly have focused on block copolymers (BCPs). Amphiphilic BCPs with immiscible blocks microphase-separate into domains in which the equilibrium domain size (typically 3-100 nm) and morphology are governed by the degrees of polymerization of each block [7], BCPs can self-assemble to form a variety of morphologies including spherical micelles, cylinders, gyroids, lamellae, vesicles, large compound micelles (LCMs), large compound vesicles (LCVs), tubules, etc. [20,38-40]. They can also create hierarchical structures, though this typically requires a polymer with multiple block types and/or complex processing [5,28,41,42]. Alternatively, copolymers with strong inter-molecular interactions may lead to interesting hierarchical structures through supramolecular associations [28].

To date, BCPs (e.g. diblock, triblock) have likely been the most prominent focus of solid state self-assembly research due to the creation of highly regular structures as well as applications such as lithography and photonics [26,43-48]. In comparison, while there are several studies on other copolymer architectures (e.g. random/statistical [9,49-52], telechelic [1,53], branched/comb [54–56], bottle-brush [57,58], star [59,60]), they barely scratch the surface about their ability to form complex, interesting nanostructures [61]. Comb copolymers feature regularly spaced side chains that are structurally distinct from the main backbone. The frequency (or density) and length of the side chains determine the overall polymer composition. In fact, by changing these two factors, the same average composition could be obtained for a given polymer, yet the polymer size, shape and the self-assembly behavior would be remarkably different [62–64]. Theoretical studies have shown that comb copolymers may self-assemble into numerous morphologies that include necklaces of star-like micelles, spherical, cylindrical, or lamellar micelles depending on side chain chemistry [65–67]. In addition, self-assembly of amphiphilic comb-like copolymers into polymeric vesicles (i.e., polymersomes) has garnered special interest [68–71] due to the hollow structure of vesicles, stimulating diverse applications such as micro/nanoreactors, drug delivery, chemical and waste transport [72, 73]. Another study leveraged the microphase separation of amphiphilic comb copolymers by forming thin film coatings on porous supports, or "selective layers", that separate small organic molecules such as dyes by size [74,75]. The comb copolymers used in the study, with hydrophobic backbones and hydrophilic poly(ethylene oxide) (PEO) side-chains, microphase separate to support bicontinuous domains of each component. The PEO domains, ~1 nm in diameter [13,75], act as effective nanochannels for the permeation of water, in addition to solutes small enough to penetrate the channels.

Zwitterions, defined as neutral molecules with equal numbers of positively and negatively charged functional groups, can easily be incorporated into amphiphilic copolymers as hydrophilic side groups [14,15,17]. The high polarity of the zwitterionic groups promotes microphase separation from a hydrophobic backbone in amphiphilic copolymers, leading to intriguing self-assembly in bulk [76–81]. Block copolymers with zwitterionic groups have been shown to form micelles in aqueous solution [82–84], yet their bulk self-assembled morphology has not been well documented. The self-assembly of zwitterionic comb copolymers (ZCCs) has not been explored despite this intriguing potential, and the evident versatility for tuning the nanostructure by changing the side chain density and length. The strong associations between zwitterionic groups [85] also indicate the likelyhood of accessing interesting morphologies.

In this study, we seek to understand how self-assembled morphologies formed by zwitterionic comb copolymers are affected by side-chain length, side-chain density, and the film formation process. Our ultimate goal is to develop selective thin films that derive their morphology and function from this self-assembled nanostructure. Most membranes are manufactured on porous supports to improve their mechanical properties. Therefore, we also explore the effect of using a porous substrate for these films. Finally, we characterize how the thin film morphology and polymer chemistry links with water permeability.

For this purpose, we synthesized a series of comb copolymers that incorporate a poly(2,2,2-trifluoroethyl methacrylate) (PTFEMA) backbone and short side-chains formed from the zwitterionic monomer sulfobetaine-2-vinyl pyridine (SB2VP) (Fig. 1A). The fluorinated PTFEMA backbone affords a high degree of hydrophobicity to the copolymer and thus chemical and physical stability in aqueous environments [86], whereas the hydrophilic, zwitterionic SB2VP side chains with uniquely high dipole moment induce phase separation, which leads to self-assembled nanostructures during film formation [85,87-89]. First, we focused on understanding how the polymer structure (architecture and composition) and film preparation method affect the self-assembled domain size and thin film morphology. For this purpose, we applied copolymers with varying zwitterionic side chain density and length as a thin film on glass substrate by two methods; spin coating and non-solvent induced phase separation (NIPS), and characterized the surface nanostructure (Fig. 1 C, D). Upon screening these self-assembled nanostructures, we chose a zwitterionic comb copolymer that yielded a nanoporous network using NIPS for further characterization. We applied this copolymer by NIPS as a thin layer on a porous membrane support to attain a mechanically supported thin film (MSTF) aimed at water transport applications. Interestingly, the use of the porous support led to a different morphology than those observed on the glass plate. In this system, self-assembly of the copolymer led to interesting hierarchical structures comprising 17 $\pm$ 5 nm spherical features in addition to larger nanopores in 85 $\pm$ 45 nm diameter range. The size of the features could be tuned by the addition of the zwitterionic homopolymer PSB2VP in the copolymer solution. These films also exhibited significant changes in water permeance and morphology upon exposure to saline solutions, which are known to lead to the expansion of zwitterionic side-chains. These results demonstrate the wide range of morphologies accessible by this family of comb copolymers, and also document the significant effect of a porous support on the film formation process. MSTFs prepared from this family of copolymers have the potential for use in many applications that leverage this nanostructure, from water treatment with enhanced selectivity to multi-functional membranes that leverage the enhanced surface area arising from the hierarchical structures.

ZCCs featuring a hydrophobic 2,2,2-trifluoroethyl methacrylate

Table 1
Free radical polymerization (FRP) reaction parameters and properties of the product P(TFEMA-*stat*-CEM) backbone copolymers.

	Reaction parameters								Copolymer properties			
Polymer name	TFEMA	CEM	AIBN	TFEMA:Cl mole ratio	DMSO	Reac. time	Reac. temp.	Yield	TFEMA:Cl mole ratio [a]	M_n [b] (g/mol)		PDI [c]
PT30	30 g	0.66 g	3 mg	36:1	100 mL	48 h	70°C	60%	30:1	3.2×10^5		2.06
PT50	30 g	0.44 g	3 mg	55:1	100 mL	48 h	70°C	70%	50:1	6.3×10^5		2.07

[a] Copolymer composition obtained using ^{1}H-NMR spectroscopy; see Appendix A for details.
[b] M_n was calculated using gel permeation chromatography (GPC) calibrated with poly(styrene) standards.
[c] Polydispersity index (PDI) reported based on GPC data.

(PTFEMA) backbone (pink) and zwitterionic sulfobetaine-2-vinyl pyridine (SB2VP) side chains (blue) were prepared with varying side chain density and length. Each copolymer was applied as a thin film on glass substrate either by (B) spin coating or (C) non-solvent induced phase separation (NIPS), where a polymer solution in trifluoroethanol (TFE) was coated onto a glass plate and then immersed in a non-solvent, isopropanol, followed by water, in an approach that mimics membrane formation and coating processes in industry. The surface nanostructure was imaged by Atomic Force Microscopy (AFM). Representative images from two of the prepared copolymers (II and IV) show that distinct self-assembly features are obtained by changing the copolymer chemistry or film preparation method.

2. Materials and methods

2.1. Materials

2,2,2-Trifluroethyl methacrylate (TFEMA) was purchased from Scientific Polymer Products Inc. (Ontario, NY). 2-chloroethyl methacrylate (CEM) was purchased from Alfa Aesar (Tewksbury, MA). Basic activated alumina, azobisisobutyronitrile (AIBN), monomethyl ether of hydroquinone (MEHQ), 2-vinylpyridine, 1,3-propanesultone, N,N,N',N'',N''-pentamethyldiethylenetriamine (PMDETA), copper (II) chloride ($CuCl_2$), L-ascorbic acid, phosphate buffered saline (PBS) were all purchased from Sigma Aldrich (St. Louis, MO). Dimethyl sulfoxide (DMSO), tetrahydrofuran (THF), toluene, ethanol, hexane, trifluoroethanol (TFE), isopropanol (IPA) and sodium chloride (NaCl) were all acquired from VWR (West Chester, PA). Deuterated dimethyl sulfoxide (DMSO-d_6) was purchased from Cambridge Isotope Laboratory (Tewksbury, MA). Monomers TFEMA and CEM were passed through a basic activated alumina column to remove any inhibitor. All other chemicals and solvents were reagent grade and used as received. PVDF400R ultrafiltration membrane used as support membrane was purchased from Nanostone Water, Inc. (Oceanside, CA).

Sulfobetaine 2-vinylpyridine (SB2VP) monomer was synthesized following the protocol reported in our previous publication [90], adapted from a previous report [91]. In brief, 2-vinylpyridine was dissolved in acetonitrile, and a slight excess of 1,3-propane sultone was added. The flask was sealed, purged with nitrogen, and stirred at 60°C for three days. The product, a light yellow precipitate, was vacuum filtered, purified by extracting in diethyl ether twice, and then dried in a vacuum oven.

2.2. Polymer synthesis and characterization

The backbone copolymer P(TFEMA-*stat*-CEM) was synthesized by the Free Radical Polymerization (FRP) of two monomers, TFEMA and chlorinated monomer CEM. TFEMA, CEM and initiator AIBN were dissolved in DMSO in a 250 mL round bottom flask. DMSO was selected due to its ability to dissolve the monomers and the copolymer. The copolymer also dissolved in THF, TFE, and other common solvents reported for PTFEMA. AIBN amount was kept low with respect to the total monomer amount (AIBN:total momoner ratio of ~1:10,000 by mass) to attain a high molecular weight copolymer product at the end. The solution was purged with nitrogen for 30 min to remove any dissolved oxygen. The reaction was stirred at 350 rpm for 48 h in an oil bath set to 70°C. To terminate the reaction at the end of 48 h, inhibitor MEHQ (1.5 g) was added, and the reaction content was exposed to air. Then, the copolymer was precipitated into a 1:1 by volume solution of ethanol: hexane, followed by three washes in ethanol, each of which involved leaving the polymer in a fresh ethanol bath overnight at room temperature, to purify the product. For drying, the copolymer was first left under the fume hood for two days and then two more days in a vacuum oven set at 50 °C. Chemical characterization was performed by ^{1}H-NMR (Bruker Avance III 500 MHz spectrometer, DMSO-d_6) d 4.90-4.35, 4.25-4.10, 3.90-3.75, 2.3-1.35, 1.30-0.5 (all broad signals; sample spectrum is shown in Fig. A1, the composition calculation procedure is detailed in Appendix A section A1.1, and integrated peak areas are listed in Table A1, Appendix A). Extended delay times of up to 10 s were typically necessary to get accurate compositions. Two batches of P(TFEMA-*stat*-CEM) were synthesized using different CEM density along the backbone, labeled PT30 and PT50, associated with the PTFEMA:CEM molar ratios of approximately 30:1 and 50:1, respectively. The very low fraction of CEM units, which leads to small peak areas for this unit, implies some error margins around these values. The copolymer properties and reaction parameters for both batches are given in Table 1. The copolymer compositions were consistent with the molar ratios used in the reaction mixture, with possibly a slight enrichment of CEM in the copolymer. These results imply that the copolymerization was likely close to random, with reactivity ratios expected to be close to 1. These values were measured at conversions around 60-70%, expected to be similar to the reported yield values because the copolymer was precipitated easily and a significant loss of product during purification was not expected. While this conversion is not as low as used in accurately determining reactivity ratios, it is still significantly below 100%. A more in-depth study of reactivity ratios, performed using a wide range of monomer ratios and low conversions, would offer deeper insight into the types of graft copolymer architectures that can be obtained using this backbone chemistry.

The homopolymer PSB2VP was synthesized by free radical polymerization of SB2VP. The SB2VP monomer is soluble in water, TFE, DMSO, and formamide. It is insoluble in dimethyl formamide, dimethyl acetamide, THF, and other non-polar solvents. First, SB2VP (10 g) was dissolved in trifluoroethanol (TFE, 60 mL) in a 100 mL round bottom flask. Then, initiator AIBN (0.02 g) was added into this solution (AIBN: total monomer ratio of ~1:500 by mass). After nitrogen purging for 30 min, the reaction was stirred at 350 rpm at 60°C for 48 h. Inhibitor MEHQ (0.5 g) was used to stop the reaction, and then the polymer was precipitated in 1:1 by volume solution of ethanol:hexane. For further purification, the homopolymer poly sulfobetaine-2-vinyl pyridine (PSB2VP) was subject to three overnight washes in ethanol, performed as described earlier. After drying, ^{1}H-NMR was employed to confirm the polymer structure, and the calculated yield was ~40%.

To synthesize the comb copolymer PTFEMA-*g*-SB2VP, Activators ReGenerated by Electron Transfer ATRP (ARGET-ATRP) was employed. The zwitterionic SB2VP side-chains, synthesized according to previous literature [92], were initiated and propagated from the chlorine atoms of CEM interspersed along the backbone. In synthesis of comb copolymers derived from the PT30 backbone, P(TFEMA-*stat*-CEM) (2 g) and SB2VP (18 g, 20 SB2VP units per CEM) were dissolved in DMSO (~

Table 2
ARGET-ATRP reaction parameters and compositions of the product ZCCs.

Polymer name	Reaction parameters				Copolymer properties			
	Reac. temp.	Reac. time	Yield	Initiation efficiency [a]	PTFEMA-*stat*-CEM backbone	Backbone: SB2VP mass ratio [b]	Cl:SB2VP mole ratio	M_n [c] (g/mol)
PT30-SB6	61°C	18 h	40%	50%	PT30	89:11 1:6		3.6×10^5
PT30-SB13	63°C	18 h	65%	40%	PT30	82:18 1:13		3.9×10^9
PT50-SB8	64°C	20 h	42%	50%	PT50	90:10 1:8		7.0×10^5
PT50-SB12	64°C	20 h	54%	30%	PT50	92:8 1:12		6.8×10^5

[a] Initiation efficiency calculated using ^{1}H-NMR; see Appendix A for details.
[b] Composition calculated using ^{1}H-NMR; see Appendix A for details.
[c] M_n was estimated using the estimate of the backbone M_n combined with the copolymer composition, and thus is a rough estimate.

80 mL) in a 250 mL round bottom flask to obtain a ~4 wt.% solution by stirring overnight at 500 rpm in an oil bath set to reaction temperature. After complete dissolution, the mixture was purged with nitrogen for one hour. In another 250 mL round bottom flask, L-ascorbic acid (0.33 g), copper (II) chloride ($CuCl_2$, 0.16 g) and PMDETA (0.5 mL) were added, and then the monomer mixture was rapidly poured into this flask. The flask was capped with a rubber septum, sealed with a zip tie and then placed back in the oil bath set at reaction temperature (see Table 2) under 360 rpm stirring. The headspace was purged with nitrogen for 20 min, and the reaction was kept running for predetermined time. To terminate the polymerization, the reaction flask was brought to room temperature, exposed to air and inhibitor MEHQ (0.19 g, 5 wt.% of the total monomer mass) was added. The reaction content was precipitated into a 1:1 by volume solution of ethanol:hexane, and collected by vacuum filtration. The solid polymer obtained was first kept overnight in ethanol to extract unreacted monomer, and then washed twice overnight by immersion in a large volume of deionized water, refreshed periodically. After filtration, the polymer was kept two days under the fume hood and two more days in vacuum oven at 50 °C for drying. PT50-derived comb copolymers were synthesized by adjusting the reaction contents according to chlorine percentage in the backbone. The copolymer composition and side-chain length were determined using ^{1}H-NMR (Bruker Avance III 500 MHz spectrometer, DMSO-d_6). In total, four batches of P(TFEMA-*g*-SB2VP) were synthesized by growing the SB2VP side chains at two different lengths from each of PT30 and PT50 backbone. The comb copolymers were encoded PT30-SB6, PT30-SB13, PT50-SB8 and PT50-SB12, with regard to the backbone used (PT30 or PT50) and the SB2VP side chain length. The properties of the product copolymers and reaction parameters are given in Table 2. These copolymers were soluble in DMSO at low concentrations, and in TFE at higher concentrations.

To estimate the molecular weight and polydispersity index (PDI) of backbone polymer P(TFEMA-*stat*-CEM), we used a Shimadzu Gel Permeation Chromatography (GPC) System equipped with a TOSOH TSK gel GMHh-M mixed-bed column and guard column, equipped with both UV and refractive index detectors. THF was used as the mobile phase at 0.75 mL min^{-1} elution rate and calibrated with low PDI poly (styrene) standards (TOSOH, PSt Quick Kit). To estimate the molecular weight of the comb copolymers, we assumed the M_n value measured by GPC was a true molar mass and calculated the total molar mass after grafting using the backbone:side-chain weight ratio. This molar mass is a rough estimate, given GPC reports a relative molar mass based on polystyrene standards. This copolymer did not dissolve in the GPC solvent. Furthermore, GPC measurements of graft copolymers are confounded by the different degrees of swelling of each component as well as the fact that side-chains change the hydrodynamic diameter in different ways than a straight chain. Therefore, the reported value is intended as an indicator of chain size.

Thermal analysis of the synthesized copolymers was performed using Differential Scanning Calorimetry (DSC). Polymer samples with a mass of ~7 mg were encapsulated in aluminum pans, and then measured in standard DSC mode using a TA Instruments Q100 DSC purged with dry nitrogen gas at a flow rate of 50 mL/min. The glass transition (T_g) temperature was measured from an endotherm acquired by heating the polymer sample at a rate of 10°C/min. The polymer sample was first equilibrated at -80°C for 5 min. Then, the temperature was ramped up to 250°C at 10°C/min. After a 5 min isothermal hold, the sample was cooled to -80°C at 10°C/min. After another isothermal hold of 5 min, it was again ramped up to 250°C at 10°C/min. The last heating cycle is reported there.

2.3. Thin film formation

The copolymer solutions for thin film formation were prepared by dissolving 3 wt.% of the copolymer in trifluoroethanol (TFE) by stirring at room temperature for 24 h. Subsequently, the solutions were filtered through 1 μm glass fiber syringe filter and kept in sealed vials overnight at room temperature for degassing. To form a thin film of the copolymer on glass substrate, we used three different methods:

1 Spin coating for 3 min at 1000 rpm.
2 Spin coating for 3 min at 1000 rpm followed by immersion in deionized water (hydration).
3 Non-solvent Induced Phase Separation (NIPS), where the solution was cast with a rolling rod (Gardco, Pompano Beach, FL) calibrated to a gap size of 6 μm, followed by air drying for 12 s, immersion in isopropanol (a non-solvent) and then immersion in deionized water.

Thicknesses of the films applied on glass substrate were measured by AFM scratch test. In mechanically supported thin film (MSTF) preparation, the 3 wt.% copolymer solutions were cast onto PVDF400R support using the rolling rod with a 6 μm gap size. After casting, the MSTF was air-dried for a predetermined time to allow solvent evaporation, and then immersed into isopropanol bath for one hour to precipitate out the copolymer by NIPS. Air drying time was applied as 5, 12 or 25 s. At the end, the MSTF was immersed and stored in a deionized water bath with antibacterial preservative sodium metabisulfite. To change the pore size and morphology of the MSTFs, we added different ratios of homopolymer PSB2VP at 10, 20 or 60 wt.% of the copolymer, where the copolymer composition was set to be 3 wt.% of the casting solution. Then, we followed the same film formation procedure using 12 s air drying preceding NIPS.

2.4. Characterization of thin film nanostructure

To study the comb copolymer self-assembly and thin film surface morphology, we performed Atomic force microscopy (AFM) measurements with a Dimension 3100 AFM (Veeco, Plainview, NY) in tapping mode. AFM cantilevers were purchased from Bruker with f_0 = 50–100 kHz and k = 1–5 N m^{-1}. Thin films deposited on glass substrate were measured as is, and the MSTFs on membrane support were taped on a glass slide after drying for the AFM measurements. The sizes of the surface features were measured using Gwyddion software and pore size distribution was obtained using ImageJ software [93] from the scanned images.

Transmission Electron Microscopy (TEM) was conducted to

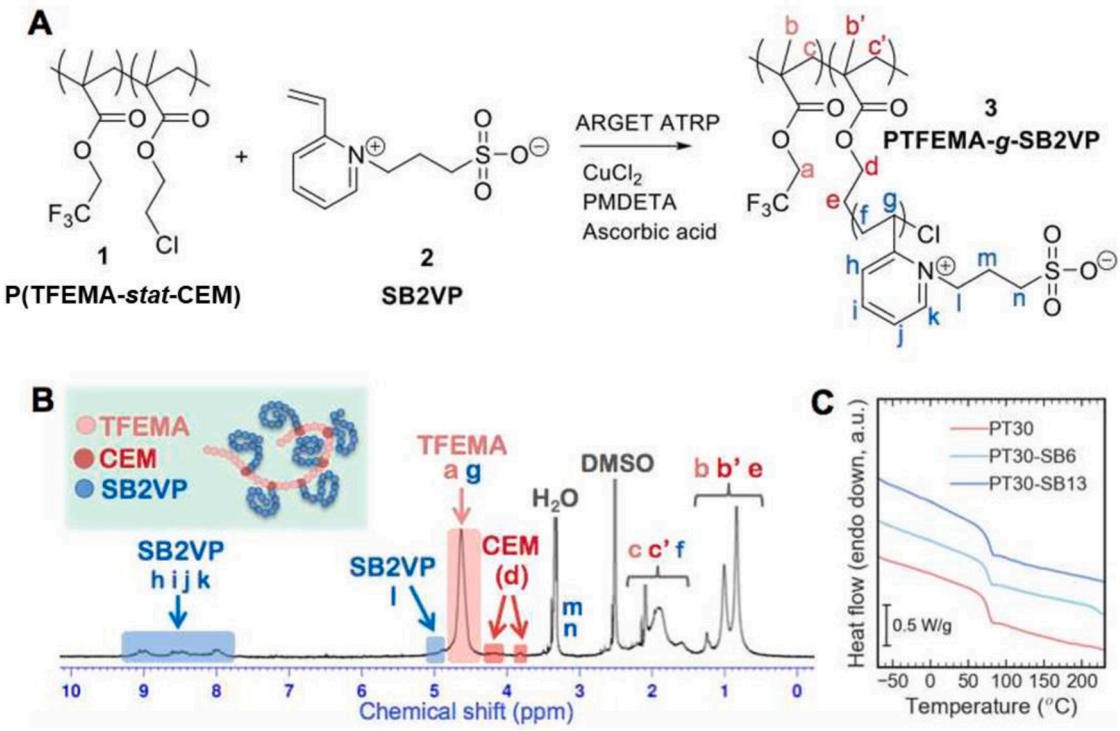

Fig. 2. (A) Synthesis scheme for the ZCC PTFEMA-*g*-SB2VP, (B) ^{1}H-NMR spectrum of the copolymer PT30-SB13, and (C) Heat flow vs. temperature of the PT30-based ZCC series at a heating rate of 10 °C/min.

characterize the self-assembled nanoscale morphology of the thin films. Images were acquired using a FEI Technai Spirit Transmission Electron Microscope in bright field mode operated at 80 keV. For sample preparation, we simulated the thin film preparation procedure by NIPS on TEM grids (200 mesh, Electron Microscopy Sciences). First, a 0.1 wt.% copolymer solution in TFE was drop-cast on the copper grid, and the solvent was allowed to air dry for 5, 12 or 25 s. Then, the grid was submerged in isopropanol for 10 min, deionized water for 10 min and dried overnight. No external staining was used. As a control, we prepared a film by air drying only without any immersion step. Feature size was measured using ImageJ software.

To image these comb copolymer coatings, serving as the selective layer of the MSTF membranes, we acquired cross-sectional images using Supra 55 FESEM at 4 keV and 10 mm working distance. In sample preparation, the MSTFs were dipped in liquid nitrogen and then cut with a clean razor blade to attain the cross section. The samples were sputter coated (Cressington 108 manual, Ted Pella Inc., CA) with gold/palladium alloy (60/40) for 120 s at 30 mA current in an argon atmosphere. The selective layer thickness was measured from the FESEM images using ImageJ software, averaged over measurements on five different sections.

2.5. Thin film permeance

Filtration experiments were performed on MSTFs with an Amicon 8010 stirred, dead-end filtration cell (Millipore) with a cell volume of 10 mL and an effective filtration area of 4.1 cm^2, connected to a 3.5 L dispensing vessel. A Scout Pro SP401 balance connected to a Dell laptop was used to automatically record the permeate weight every 30 s using TWedge 2.4 software (TEC-IT, Austria). Prior to permeance tests, the MSTF was stabilized by filtering deionized water for two hours at 10 psi (0.07 MPa) pressure. After stabilization, the permeance was measured at 10 psi (0.07 MPa) pressure using a cell stirred at 500 rpm. Ionic strength responsive permeance tests were conducted using sodium chloride solutions with different concentrations (0-1 M) in deionized water.

3. Results and discussion

3.1. Synthesis and characterization of the ZCCs

Comb-shaped zwitterionic copolymers with poly(2,2,2-trifluoroethyl methacrylate) (PTFEMA) backbone and side-chains formed from sulfobetaine-2-vinyl pyridine (SB2VP), named PTFEMA-*g*-SB2VP, were synthesized using a two-step process. First, the backbone copolymer, or macroinitiator, was synthesized by the Free Radical Polymerization (FRP) of 2,2,2-trifluoroethyl methacrylate (TFEMA) and the chlorinated monomer 2-chloroethyl methacrylate (CEM). Two batches of this copolymer, P(TFEMA-*stat*-CEM), were synthesized, with different CEM density along the backbone. These were labeled PT30 and PT50, associated with the PTFEMA:CEM molar ratios of 30:1 and 50:1, respectively (Table 1) and integrated peak areas (Table A1, Appendix A). Copolymer composition, characterized using ^{1}H-NMR spectroscopy, was similar to the monomer composition used in the reaction mixture (Fig. A1, Appendix A). The resultant compositions were consistent with the molar ratios used in the reaction mixture with possibly a slight enrichment of CEM in the copolymer. These results imply that the copolymerization was likely close to random, with reactivity ratios expected to be close to 1.

The molecular weight of each P(TFEMA-*stat*-CEM) copolymer was estimated by conducting gel permeation chromatography (GPC) of the copolymers in tetrahydrofuran (THF). PT30 had a number-averaged molar mass M_n of 3.2 × 10^5 g/mol based on polystyrene standards and a polydispersity index (PDI) of 2.06, whereas PT50 had an M_n of 6.3 × 10^5 g/mol and a PDI of 2.07. These values are reasonable for free radical copolymerization systems. The difference in molecular weights could be associated with a decrease in initiator concentration at increased conversions observed for PT50. We did not expect this difference in molar masses to significantly change the resultant self-assembled morphologies. The copolymer properties and reaction parameters for both batches are given in Table 1.

To synthesize the comb copolymer PTFEMA-*g*-SB2VP, Activators

Table 3
Film thicknesses from ZCC solutions in TFE deposited on glass substrate.

Film prep. method	Film thickness (μm) PT30-SB6	PT30-SB13	PT50-SB8	PT50-SB12
Spin coat.	0.9 ± 0.05	0.9 ± 0.04	1.3 ± 0.04	1.4 ± 0.06
Spin coat. + hydration	1.2 ± 0.06	1.1 ± 0.08	1.5 ± 0.03	1.5 ± 0.08
NIPS	1.5 ± 0.07	1.5 ± 0.05	1.9 ± 0.07	2.1 ± 0.08

ReGenerated by Electron Transfer ATRP (ARGET-ATRP) was used to initiate the polymerization of zwitterionic SB2VP from the chlorine atoms on the CEM units in P(TFEMA-*stat*-CEM) (Fig. 2A) [94,95]. The zwitterionic monomer SB2VP was synthesized using previously reported protocols [92]. SB2VP side-chains were grown at two different lengths from each backbone. This resulted in four batches of comb copolymers with average zwitterionic side-chain lengths ranging between 6 and 13 repeat units. These ZCCs were labeled PT30-SB6, PT30-SB13, PT50-SB8 and PT50-SB12, the first denoting the backbone used (PT30 or PT50) and the second indicating the average SB2VP side-chain length. The compositions of these copolymers and reaction parameters used in their synthesis are given in Table 1. All samples used in this study were purified by extraction in deionized water to remove water-soluble fractions, which would be detrimental to the thin films when they are immersed in water. When we synthesized copolymers with longer reaction times to access longer side-chain lengths and/or higher SB2VP contents, a large fraction of the copolymer was lost during extraction with water. This indicates that PTFEMA-*g*-SB2VP copolymers that contain as much as 85 wt.% of the very hydrophobic monomer TFEMA can be water soluble. This may arise from the formation of micelles in water, driven by the molecular structure of the comb-shaped polymers that positions the hydrophobic segments at the core of the molecule, surrounded by highly hydrophilic zwitterionic groups. This outcome may be interesting for various applications, from drug delivery to the stabilization of emulsions.

A sample ^{1}H-NMR spectrum is shown in Fig. 2B, along with peak assignments. All peaks with chemical shifts greater than 7 ppm were assigned to SB2VP units (h i j k), with four protons per SB2VP unit appearing in that region [92]. The peak at 4.6 ppm was attributed to the convolution of CH_2 protons from TFEMA (a) and SB2VP (g). The ratio of these peaks, together with the TFEMA:Cl ratio from the composition of P(TFEMA-*stat*-CEM) used as the macroinitiator, were used to calculate the final comb copolymer composition. The percentage of chlorine atoms that initiated ARGET-ATRP (Table 2) was obtained from the ratio between the CEM peaks at 3.8 and 4.2 ppm, attributed to the unreacted and total CEM contents, respectively. To estimate the molecular weights of ZCCs (Table 2), we used the number-averaged molecular weight of each backbone obtained from GPC, and the backbone:side-chain weight ratio of each associated comb copolymer. All four copolymers had molecular weights above 10^5 g/mol.

Differential scanning calorimetry (DSC) can be used to obtain information on microphase separation in copolymers. Phase separated copolymers show two distinct glass transition temperatures (T_g) associated with each microphase, whereas a composition-dependent single T_g in a copolymer indicates lack of phase separation [96]. The T_g also affects various kinetic aspects of self-assembly such as micelle stability. For instance, glassy blocks of polystyrene in a copolymer lead to very stable micelles that are kinetically restrained at room temperature, often termed 'frozen micelles' [97]. This may enable the preservation of meta-stable morphologies formed during the formation of the thin film by limiting chain mobility once the film is formed and solidified [9]. Therefore, we characterized the thermal properties of the copolymers synthesized for this study using DSC. Fig. 2C shows the DSC thermograms from reversible heat flow versus temperature plot for the PT30 backbone and the ZCCs derived from it. We could not observe the T_g of homopolymer PSB2VP, reported to be 250 °C from previous reports [15,98,99], because it was close to or above the degradation temperature of the ZCCs. On the other hand, all copolymers showed a T_g at around 80 °C, similar to that of the homopolymer PTFEMA obtained from previous literature [15,100,101]. The observed T_g of the ZCC is identical to that of the backbone. Analogous findings were observed with the ZCCs derived from the PT50 backbone (Fig. A3, Appendix A). These results are consistent with the ZCCs microphase separating to form separate PTFEMA and SB2VP domains.

3.2. Thin film preparation on glass substrates to study the ZCC self-assembly

The morphology of thin films depend not only on the molecular parameters of the copolymers but also on the film formation process, substrate surface chemistry, film thickness, and annealing conditions [11,26]. Each of these parameters can be utilized to access new morphologies. In this study, we focused on the film formation procedure. Most BCP thin films studied in the literature are formed by spin coating, occasionally followed by an annealing step. However, spin coating is not scalable to roll-to-roll systems. This limits their use in large scale manufacture of membranes and other products. Instead, NIPS, known for its scalability, enables film formation by casting a polymer solution on solid substrate followed by immersion in a non-solvent bath to precipitate out the polymer as a film [102]. We wanted to study how this copolymer self-assembled under these two conditions, and to characterize how interactions with water further modifies the observed surface morphology. Therefore, we applied the 3 wt.% ZCC solution in trifluoroethanol (TFE) as a thin film on a glass substrate by three different methods: (1) spin coating; (2) spin coating followed by immersion in deionized water (hydration); and (3) a process that simulates NIPS method used for preparing thin film composite membranes from zwitterionic copolymers [14,15]. In the NIPS process (method 3), we spread the polymer solution onto a glass substrate by a rolling rod set to a gap size of 6 μm. This thickness is much higher than that deposited by spin coating in Method 2. After air drying for 12 s, we immersed the coated glass into an isopropanol bath, and then moved it to a bath of deionized water. We expect that the film still contained some TFE at the time when it was immersed in the non-solvent, as expected in NIPS. All thicknesses were measured by AFM scratch tests. Films prepared using this method were 0.9-2.1 μm in thickness (Table 3). Spin coated films were in general thinner than those cast by NIPS.

The Atomic Force Microscopy (AFM) images (Fig. 3) of the comb copolymer thin films on glass substrates demonstrate the dependence of the surface morphology on both copolymer chemistry and deposition procedure. The films were fairly smooth and nearly featureless when prepared by spin coating (Fig. A4, Appendix A). This changes upon the hydration of the film by immersion in water (Fig. 3, top row), which selectively swells the zwitterionic side-chain domains. Depending on zwitterionic side-chain density and length, we observed a variety of self-assembled surface morphologies. The PT30-SB6 copolymer, which had the lowest zwitterionic monomer content, remains essentially featureless after hydration. Its longer side-chain counterpart PT30-SB13 shows a disordered nanoscale pattern. The SB2VP content of the copolymer PT50-SB8 is comparable with PT30-SB6; it has less frequent yet longer side-chains. This copolymer exhibits a partially connected network of short rod-like structures with an average diameter of 26 ± 5 nm. Its longer side-chain counterpart, PT50-SB12, displays a combination of similar morphologies with interspersed spherical features, possibly micelles, 15 to 40 nm in diameter. This last finding aligns with the hypothesis that zwitterionic side-chain length is a driver for the self-assembled morphology. The observed bimodal morphology possibly stems from molecular populations with different average side-chain lengths. The high water solubility of polymers with longer side-chain lengths, observed in preliminary experiments, also supports this possibility.

AFM phase images of the films formed by NIPS (Fig. 3, middle row) display interesting nanoscale patterns on the surface. PT30-SB6 and

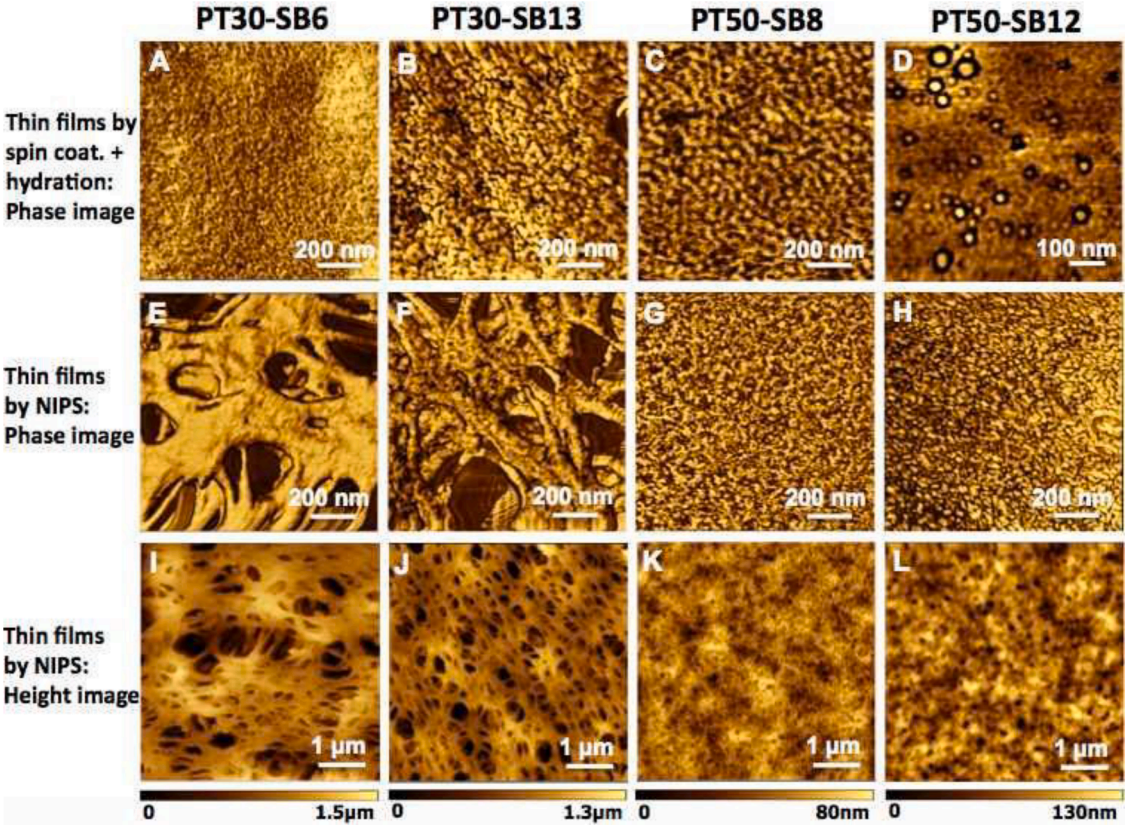

Fig. 3. (Top row, A-D) AFM phase images from 1 × 1 μm^2 surface sections of thin films deposited by spin coating the ZCC solution in TFE on glass substrates followed by hydration. (Middle row, E-H) AFM phase images from 1 × 1 μm^2 surface sections of thin films deposited by a method simulating the NIPS process for manufacturing thin film composite membranes. The ZCC solution in TFE was coated on a glass substrate using a rolling rod, air dried for 12 s, immersed in isopropanol and moved to deionized water. (Bottom row, I-L) AFM height images from 5 × 5 μm^2 surface sections of the thin films shown in middle row. Film preparation method (on left of each row) and ZCC used (on top of each column) are indicated. All AFM images were acquired in dry state.

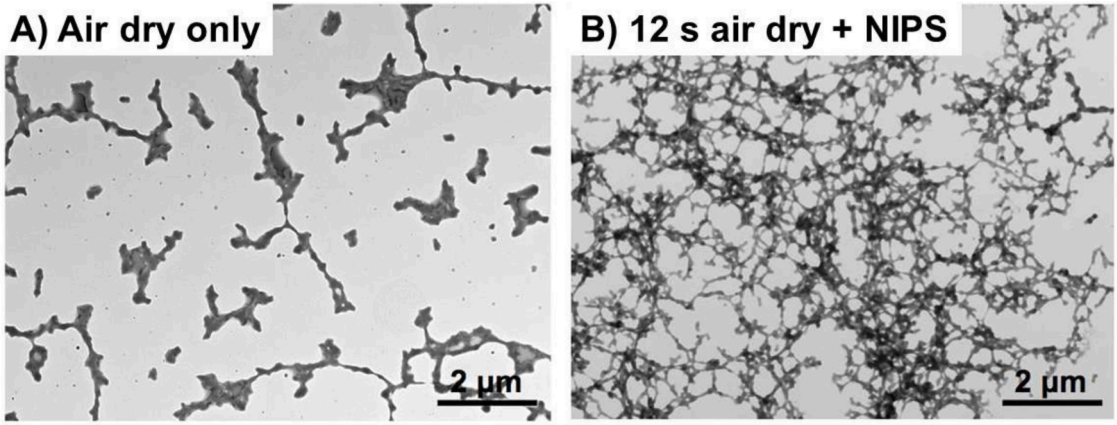

Fig. 4. TEM images of thin films deposited by drop casting 0.1 wt.% ZCC solution in TFE on the grid followed with (A) air drying only, (B) air drying for 12 s followed by NIPS in isopropanol and immersion in deionized water.

PT30-SB13 thin films exhibit porous structures formed from networks of tubules, 95 ± 20 and 55 ± 12 nm in diameter, respectively. These morphological differences between copolymers with the same side-chain density but different SB2VP content arise not only from the self-assembled morphology of polymer chains, but also from the complex interplay between solvent and non-solvent transport, as well as differences in their phase diagrams. This phenomenon is well-studied in the field of polymer membrane manufacture. The higher zwitterion content of PT30-SB13 likely leads to a difference in the time to precipitation upon contact with water, further complicating structure formation. Interestingly, PT50-SB8 and PT50-SB12 thin films show a very different self-assembly pattern. The surfaces appear somewhat porous, but the features are much smaller. This morphology is consistent with a disordered bicontinuous network, though more detailed characterization is needed to better understand this structure. The difference likely arises from the larger spacing between the zwitterionic side-chains and the higher hydrophobic backbone content. AFM height images from larger sections of the same films (Fig. 3, bottom row) are also consistent with a continuous network morphology. SEM imaging with controlled tilt, combined with image processing, may potentially offer further insight

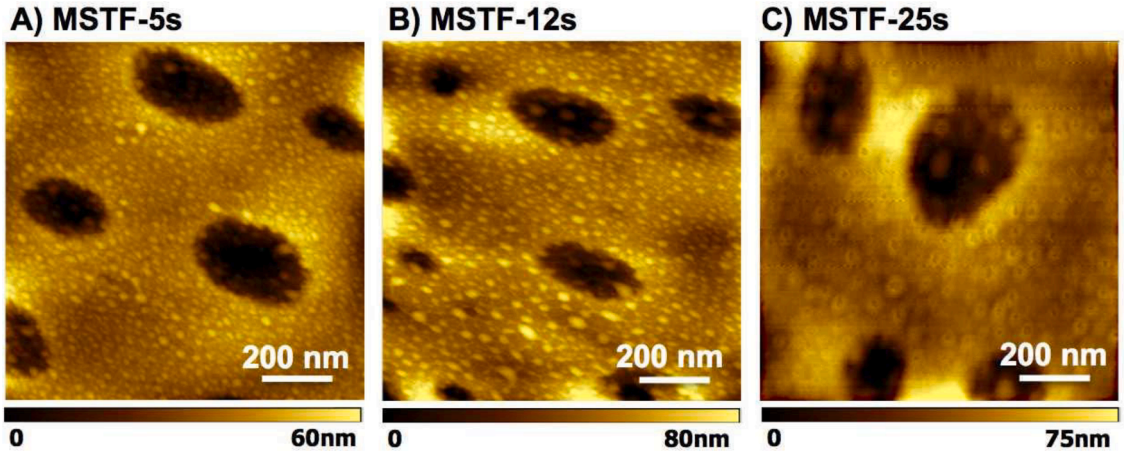

Fig. 5. AFM height image from 1 × 1 μm^2 surface section of (A) MSTF-5s, (B) MSTF-12s, and (C) MSTF-25s.

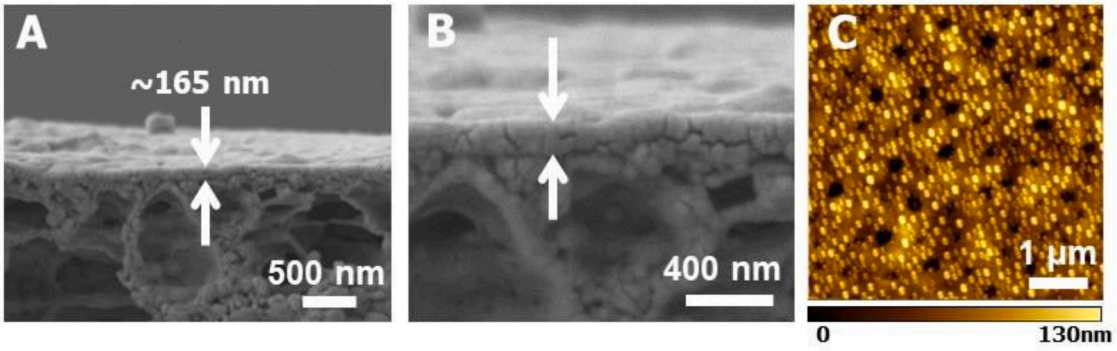

Fig. 6. (A, B) Cross-sectional FESEM image of the MSTF-12s; (B) shows a digital zoom of the selective layer. (C) AFM height image from 5 × 5 μm^2 surface section of MSTF-12s with a 130 nm z-range, showing distinct hierarchical features comprising 17 ± 5 nm spherical micelles together with larger pores of 85 ± 45 nm diameter on average. The micelle size was measured using the z-direction in AFM image because x- or y-direction may not be reliable due to tip broadening effect.

Table 4
Casting solution content, film thickness, estimated pore diameter, pore depth, center-to-center distance between pores, pore density and water permeance of the MSTFs.

Property	MSTF-12s	MSTF-PSB10	MSTF-PSB20
Casting solution composition in TFE	3 wt.% ZCC	3 wt.% ZCC 0.3 wt.% PSB2VP	3 wt.% ZCC 0.6 wt.% PSB2VP
Film thickness (nm)[a)]	165 ± 10	125 ± 11	140 ± 13
Estimated pore diameter (nm)[b),c)]	85 ± 45	92 ± 54	144 ± 81
Estimated pore depth (nm)[b),d)]	20 ± 10	21 ± 5	58 ± 10
Center-to-center distance between pores (nm)[b)]	637 ± 153	315 ± 75	562 ± 90
Pore density (x10^{12} pores m^{-2})[b)]	3.3	10	4.3
Water permeance (L m^{-2} h^{-1} bar^{-1})	93 ± 8	48 ± 4	66 ± 2

a) Obtained from cross-sectional FESEM images in dry state (Fig. 6A and Fig. S6D, E).
b) Obtained from surface AFM images in dry state (Fig. 7).
c) Obtained from x- and y-direction in AFM image and likely overestimated due to tip broadening effect.
d) Obtained from z-direction in AFM image

into this morphology. PT30-SB6 and PT30-SB13 thin films show larger pores, likely due to higher frequency in the placement of zwitterionic side-chains along the backbone in comparison with PT50-SB8 and PT50-SB12 copolymers. These findings altogether are significant in explaining the relationship between ZCC chemistry and self-assembled thin film properties, and demonstrate the diversity of variables that can be scanned for desired properties. For this specific work, we chose copolymer PT30-SB13 for further study due to its potential functionality as a porous selective layer for water transport applications. We hope to explore other copolymer compositions in future studies for other targeted applications.

The interconnected network structure formed by PT30-SB13 during the NIPS procedure is quite distinct from the structure formed by spin coating. We hypothesized that the interaction between the copolymer with isopropanol and water during the NIPS process led to the formation of supramolecular assemblies between the copolymer chains, leading to the interconnected network structure. To test this hypothesis, we simulated the thin film formation process by NIPS on Transmission Electron Microscopy (TEM) grids. First, a dilute ZCC solution in TFE was drop-cast on the grid. The solvent was allowed to air dry for a predetermined period of time, followed by isopropanol immersion for 10 min, and then water immersion for 10 min to kinetically "freeze" the structure. Self-assembly of amphiphilic copolymers in solution may evolve with the progression of solvent evaporation. This may lead to significant changes in resultant film morphology. Other groups have employed careful control of the drying time and solvent volatility to create nanostructured selective layers with interesting and highly variable functionality [8,26,101]. To explore this parameter, films were prepared with varying drying times of 5 s, 12 s, or 25 s. As a control, one film was prepared by air drying only without any immersion step. TEM images (Fig. 4) show that a network of tubular polymer structures develops when NIPS procedure is undertaken. The average diameter of these tubules was determined to be 51 ± 8 nm, comparable to the 55 ±

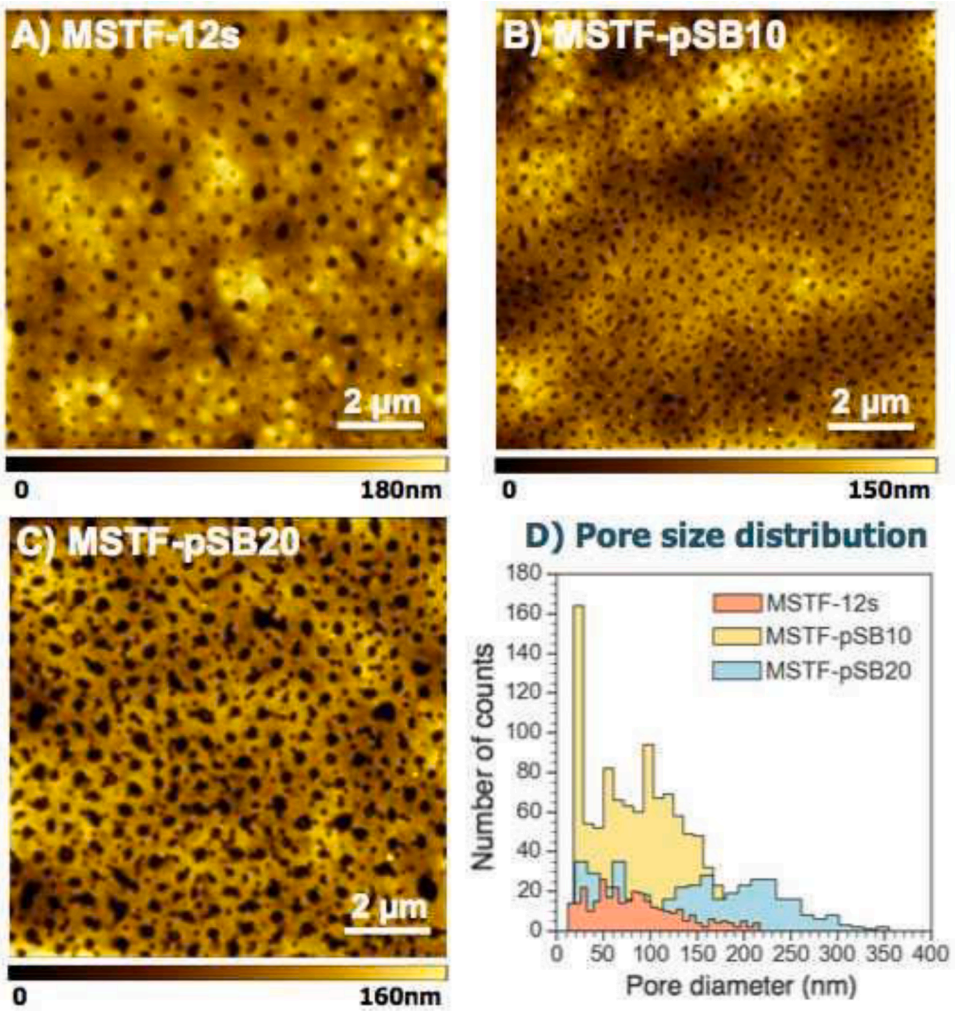

Fig. 7. AFM height image from 10 × 10 µm^2 surface section of (A) MSTF-12s, (B) MSTF-PSB10, and (C) MSTF-PSB20; (D) pore size distribution of the MSTFs calculated from the AFM images using ImageJ.

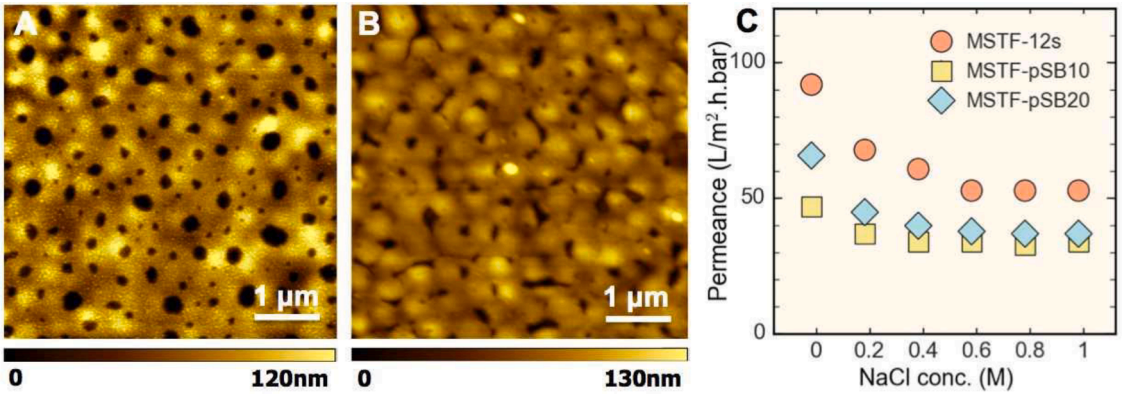

Fig. 8. AFM height image from 5 × 5 µm^2 surface section of (A) MSTF-12s, (B) MSTF-12s after overnight immersion in PBS (0.01 M, pH 7.4) followed by water immersion, and (C) plot of Permeance vs. NaCl concentration.

12 nm diameter attained from the AFM image (Fig. 3J). In contrast, air drying leads to sparse, segregated clusters of spherical enclosures, a few of which are connected by short rod-like structures. This finding emphasizes the importance of the thin film formation procedure on nanoscale structure formation. Particularly in this system, slower kinetics are afforded by slow exchange rate between the solvent TFE and non-solvent isopropanol, which allows for the development of the highly connected networks. It should be noted that we did not observe an evident change in film morphology by TEM when varying the drying time to 5 or 25 s (Fig. A3, Appendix A).

Table A1
Integrated peak areas from the ^{1}H-NMR spectrum of each backbone copolymer.

Peak	Chemical shift (ppm)	Integrated area under the peak	
		PT30	PT50
a	4.60	1	1
d	4.18	0.036	0.022
e	3.80	0.033	0.020

Table A2
Integrated areas of the relevant ^{1}H-NMR peaks.

Polymer name	Initiation efficiency (*i*)	Integrated area under the peaks	
		a, g, l (4.4–5.1 ppm)	h, i, j, k (7.8–9.2 ppm)
PT30-SB6	50%	6.1	1
PT30-SB13	40%	3.6	1
PT50-SB8	50%	6.9	1
PT50-SB12	30%	7.8	1

3.3. *Self-assembly of the ZCC on a porous support and formation of MSTF*

Most studies of polymer self-assembly focus on either free standing films or thin layers manufactured on non-porous supports, similar to those described above. Yet, when these morphologies are of interest as membrane selective layers, these manufacturing methods become impractical. Free-standing films are either too thick to allow high enough flux through them, or too thin to withstand the pressures involved in filtration operations. Films prepared on non-porous substrates have to be removed from this support and often moved onto a porous one to be used in filtration testing. This is often an arduous process that is difficult if not impossible to scale up. Instead, most studies that explore novel polymers as membrane selective layers use thin film composite membranes where the thin polymer film is supported by a mechanically robust, porous layer. These supported membranes are prepared by coating the functional polymer onto a porous support, often a commercial membrane with large pore size. However, when a coating and self-assembly process that was studied on a non-porous substrate is translated onto a porous support, the resultant layer morphology may change. Capillary forces may cause the solvent to be absorbed into the support, changing the thermodynamic and transport processes that occur during the NIPS process. This effect is even more significant if the pore size of the support is smaller than the size of polymer coils or assemblies in solution. In such a case, as the solvent is absorbed into the support, the polymer chain concentration in the liquid film coating is increased. When the membrane is immersed in a non-solvent, the selective layer will form only on top of the membrane, but effectively from a layer whose thickness and composition will be different than if the same solution was deposited on a non-porous substrate. This leads to changes in morphology, pore size, feature/pore size, and other factors. This premise has not, to our knowledge, been systematically explored.

Therefore, we wanted to better understand how the use of a porous substrate in the NIPS process to create a mechanically supported thin film (MSTF) would affect the self-assembled layer morphology of ZCCs. We prepared MSTFs from the PT30-SB13 ZCC using the NIPS process described above, replacing the glass substrate with a commercial PVDF400R ultrafiltration membrane as the porous support (see Fig. A6, Appendix A). Similar to the procedure above, a 3 wt.% solution of the copolymer in TFE was spread onto the support with a rolling rod at a gap size of 6 μm. The MSTF was air dried for a predetermined period of time. Three air drying time periods were screened, 5, 12 or 25 s, and the corresponding MSTFs were encoded MSTF-5s, MSTF-12s, and MSTF-25s, accordingly. Then, the coated membrane was immersed into an isopropanol bath for one hour to precipitate out the copolymer. Finally, the MSTF was immersed and stored in a water bath.

The surface morphologies of these MSTFs were characterized by AFM. Close examination of the thin film surfaces display interesting, hierarchical features; we observe, in addition to the pores, small spherical features, likely attached frozen micelles, covering the surface (Fig. 5). The size and density of these smaller features appear to increase with increasing drying time. Lower magnification/larger area imaging of the surface morphology of the MSTFs displayed a macroporous structure with pores ~30-200 nm in diameter, spread randomly across the surface (Fig. A7, Appendix A). Porous materials that feature hierarchical structures ranging between nano to macroscopic scales are intriguing because they afford high flux and pore accessibility together with high surface area [5,28,41]. These are highly demanded characteristics in separation, membrane chromatography, catalytic conversions, detection, energy conversion and storage, to name a few. Most processes for attaining hierarchically structured materials are multi-stage and tedious [103]. Instead, the hierarchical features of the MSTFs in this study develop spontaneously, with no added manufacturing steps.

Water permeation tests showed permeances of 75 ± 5, 93 ± 8 and 29 ± 3 L m^{-2} h^{-1} bar^{-1} for the MSTFs formed using 5, 12 and 25 s drying times, respectively. These results suggest that controlled solvent

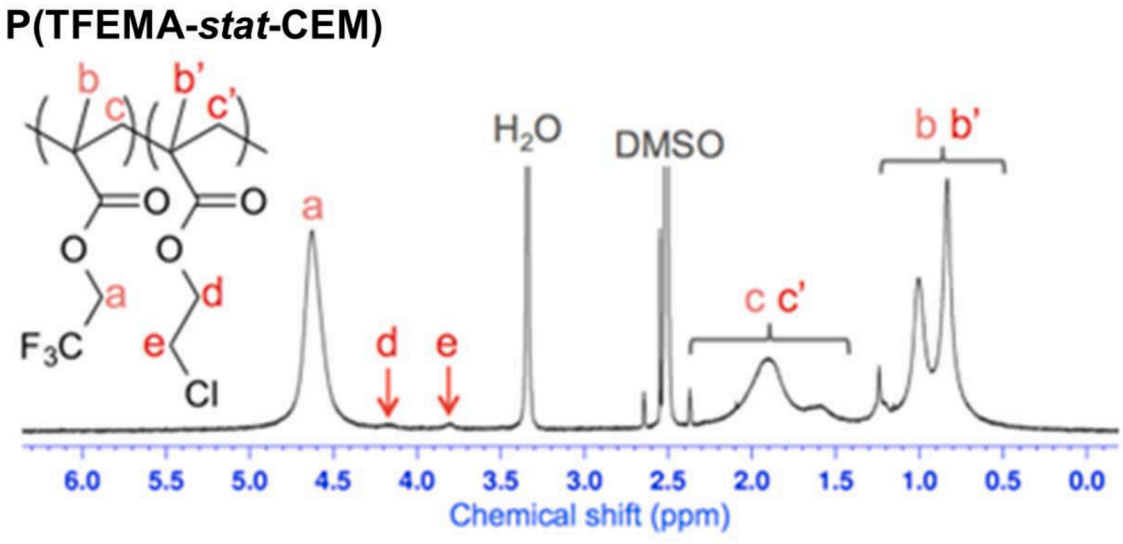

Fig. A1. ^{1}H-NMR spectrum of the backbone copolymer P(TFEMA-*stat*-CEM) labeled PT30.

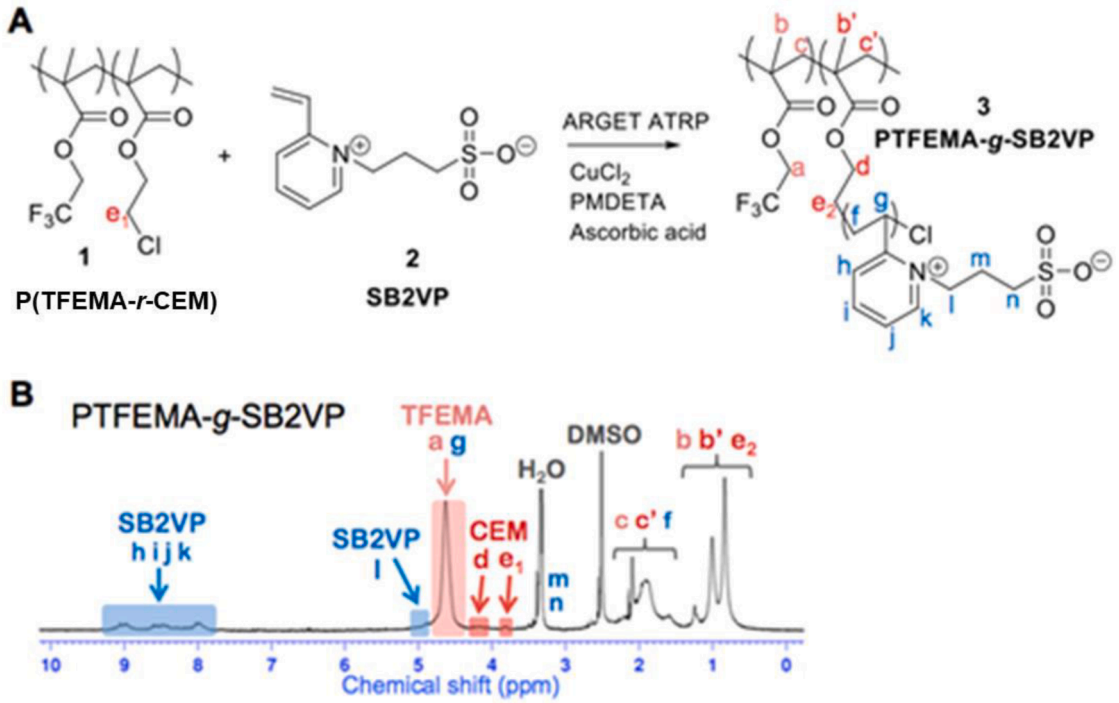

Fig. A2. (A) Synthesis scheme for the ZCC PTFEMA-*g*-SB2VP, (B) ^{1}H-NMR spectrum of the copolymer PT30-SB13.

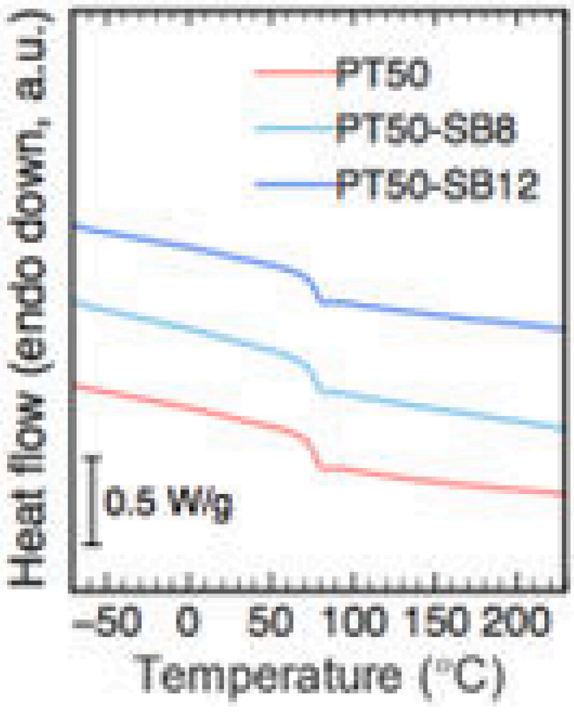

Fig. A3. Heat flow v.s. temperature of the PT50-based comb copolymer series at a heating rate of 10 °C/min.

evaporation prior to phase inversion affects selective layer permeability. This may arise due to evolving self-assembly during solvent evaporation from the solution-air interface. Although AFM images indicated that the pores seemingly became larger with increasing solvent evaporation time, the lowest permeance was observed in MSTF-25s with the longest evaporation time. This may be a consequence of pores not percolating the entire thickness of the film. Alternatively, the longer evaporation time may lead to some of the copolymer entering into the inner pores of the support membrane through capillary forces, clogging them up. Variations in permeance may also arise from differences in film thickness and/or overall layer porosity. In general, further in-depth studies with larger sample sizes and more controlled environments would be needed for deeper conclusions. Among the MSTFs prepared, we chose to conduct a more thorough analysis of MSTF-12s because it showed the highest permeance.

To determine the film thickness of MSTF-12s, we acquired a cross-sectional FESEM image (Fig. 6A-B) and analyzed it in comparison with the cross-sectional FESEM image of the uncoated porous support (Fig. A6A, Appendix A). The ~165 nm thick film layer of MSTF-12s adheres well to the support membrane through partial penetration of the copolymer into support membrane pores via intermolecular interactions.

A detailed visual from the 5 × 5 μm^2 surface section of MSTF-12s (Fig. 6C) allows better visualization of the distinct hierarchical features comprising 17 ± 5 nm spherical features together with larger pores of 85 ± 45 nm diameter. The spherical feature size was measured using the z-direction in AFM image because x- or y-direction may not be reliable due to tip broadening effect. While there are limitations to calculating pore sizes by AFM (e.g. identifying pores versus peak and valley structures), previous studies have shown AFM data to be consistent with membrane pore sizes calculated from rejection curves [104]. Further in-depth SEM analysis can potentially offer further insight into pore size distributions. We also performed a radially integrated FFT on the AFM image in Fig. 6C, however we did not observe an order in packing. These features are not present in a similar thin film formed on a non-porous silicon wafer substrate using the same procedure (Fig. 3J). The absence of the spherical <30 nm features on this film confirms that a porous substrate is required for inducing the desired hierarchical morphology. Observed with each drying time in MSTF-12s, this hierarchical morphology is interesting because it increases the roughness and interfacial area of the materials, which may have exciting outcomes that alter wettability, permeability, selectivity, fouling, and hydrodynamic resistance to flow across the film surface. In addition, the high surface area may be interesting for further functionalization to create

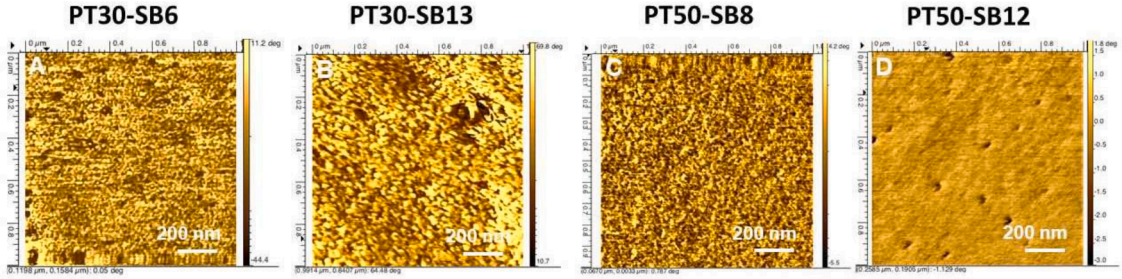

Fig. A4. AFM phase images from 1 × 1 μm^2 surface sections of thin films deposited by spin coating the 3 wt.% copolymer solution in trifluoroethanol (TFE) on a glass substrate. Comb copolymer used is indicated on top of each image.

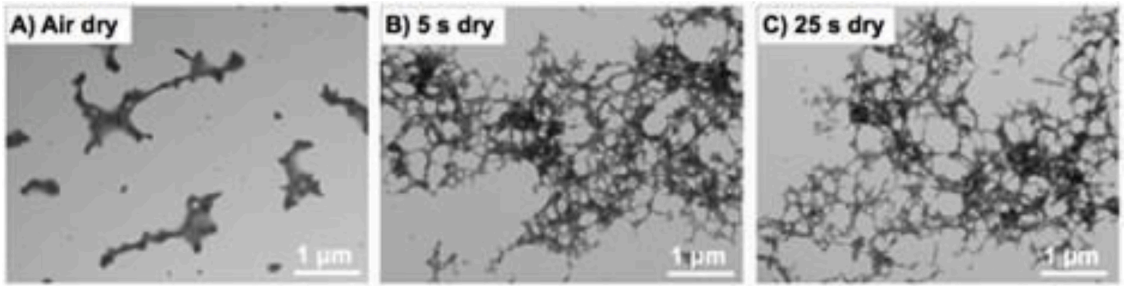

Fig. A5. TEM images of thin films deposited by drop casting 0.1 wt.% zwitterionic comb copolymer solution in TFE on the grid followed with (A) air drying, (B) air drying for 5 s, NIPS in isopropanol and immersion in deionized water, and (C) air drying for 25 s, NIPS in isopropanol and immersion in deionized water.

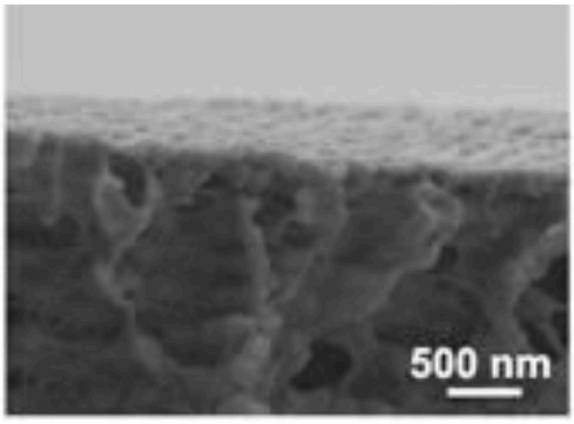

Fig. A6. Cross-sectional FESEM image of the PVDF400R support.

multi-functional membranes or membrane adsorbers.

3.4. Modifying the nanostructure of MSTF with a zwitterionic homopolymer additive

While the copolymer architecture and composition is a powerful tool for controlling the self-assembled morphology, it is often impractical to synthesize a new copolymer for each targeted application. This has led us to explore the use of additives to further modify the morphology of MSTFs prepared by this zwitterionic comb copolymer. Studies that focus on self-assembling block copolymers show that blending the copolymer with a component that preferentially segregates into one domain over another can modify its domain size and morphology [26]. This principle has been applied to membrane manufacture to tune the pore size [43, 105-107]. For instance, mixing poly(styrene)-*block*-poly(methyl methacrylate) (PS-*b*-PMMA) copolymer with PMMA homopolymer leads to enlarged PMMA domains. The homopolymer can then be dissolved away in a selective solvent to leave behind pores [106]. The pore size and morphology can be tuned by changing the blend composition [107]. Block copolymer self-assembly has also been integrated into membrane manufacture through an approach termed Self-assembly-Non-solvent Induced Phase Separation (SNIPS) [43], where the use of additives that partition into and at times order one domain can alter domain structure [108–111]. We chose to adapt this simple, scalable approach to modify the pore size and morphology of MSTF-12s. During film formation, we added different ratios of homopolymer poly (sulfobetaine-2-vinyl pyridine) (PSB2VP) into the PT30-SB13 copolymer solution in TFE, and then followed the film formation procedure identical to that of MSTF-12s. We added 10, 20 or 60% of the amount of the ZCC PT30-SB13, with the ZCC composition set to 3 wt.% of the casting solution. The resulting MSTFs were encoded MSTF-PSB10, MSTF-PSB20 and MSTF-PSB60, respectively (Table 4).

The surface AFM images of MSTFs prepared using this additive are morphologically different than those prepared without the homopolymer (Fig. 7). The addition of 10 wt.% PSB2VP with respect to the copolymer PT30-SB13 (MSTF-PSB10) led to tripled pore density and an average pore size of 92 ± 10 nm, calculated from image analysis of the AFM images. The cross-sectional thin film structure was similar for all the MSTFs, indicated by FESEM images (Fig. A8, Appendix A), with thicknesses between 120 and 170 nm (Table 4). On the other hand, water permeance (Table 4) was cut down nearly to half that of additive-free MSTF-12s. This may potentially be due to an increased number of pores that do not percolate through the entire film. Alternatively, it may also relate to the broad distribution of pore sizes in this MSTF, where the large pores are responsible for the high flux through the membrane. Increasing the PSB2VP content further to 20 wt.% of the copolymer mass (MSTF-PSB20) resulted in significantly larger pores with an average diameter of 144 ± 81 nm, and moderately improved the water permeance compared to MSTF-PSB10. At 60 wt.% PSB2VP content with respect to the copolymer (MSTF-PSB60), pores became large with distorted morphology (Fig. A9, Appendix A), and thus further analysis was not performed on the AFM image. Water permeance was measured to be 62 ± 5 L m^{-2} h^{-1} bar^{-1}, showing no increase compared to that of MSTF-PSB20. We should note that, similar to additive-free MSTF-12s, all PSB2VP-added thin films showed hierarchical morphology with

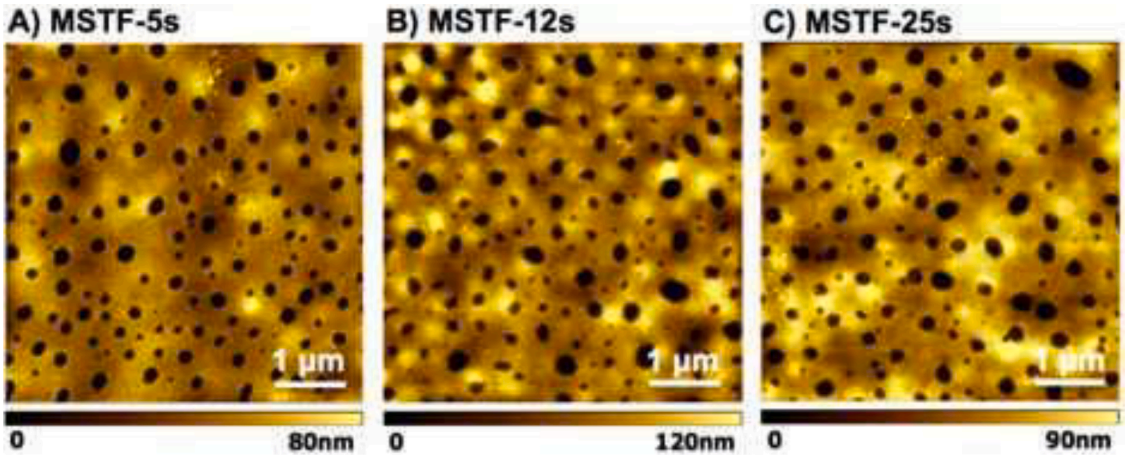

Fig. A7. AFM images of the MSTFs prepared by casting the 3 wt.% copolymer solution in TFE on porous PVDF400R support followed with air-drying for a predetermined time, NIPS in isopropanol and immersion in deionized water. AFM height image from 5 × 5 μm^2 surface section of (A) MSTF-5s prepared by air-drying for 5 s, (B) MSTF-12s prepared by air-drying for 12 s, and (C) MSTF-25s prepared by air-drying for 25 s prior to NIPS. MSTF code is indicated on top of each column. All the MSTFs show a macroporous surface with pores spread randomly across the surface and smaller spherical micelles covering the nonporous sections of the surface.

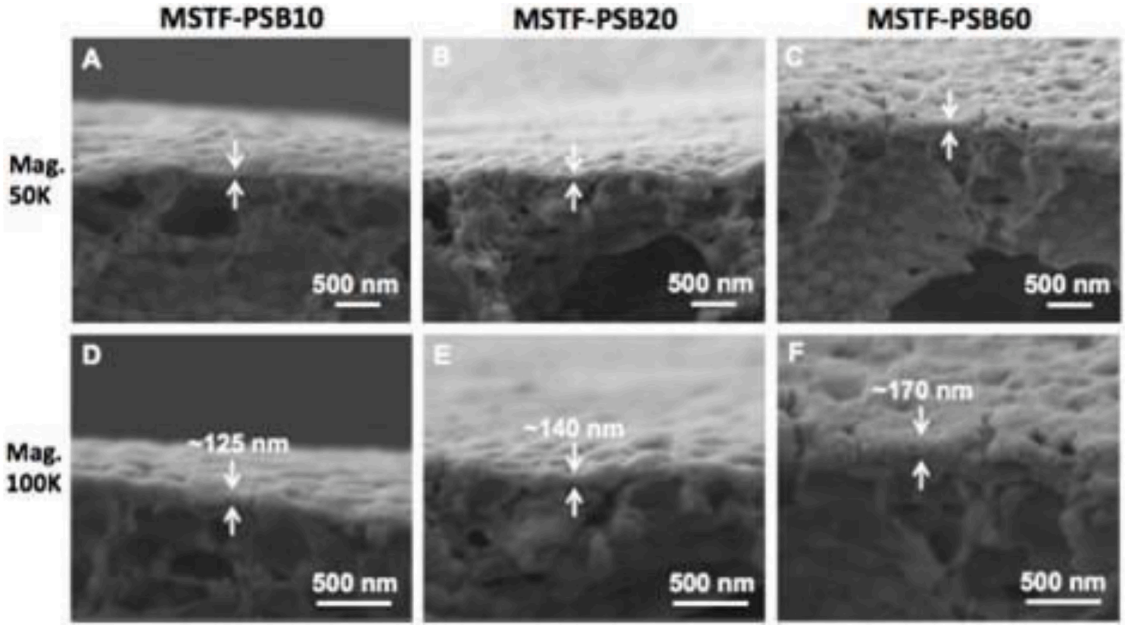

Fig. A8. Cross-sectional FESEM images of the mechanically supported thin films (MSTFs) prepared using homopolymer PSB2VP additive fixed at 10, 20 or 60 wt.% of the copolymer PT30-SB13, where the PT30-SB13 composition was set to be 3 wt.% of the casting solution. The MSTFs are encoded based on the additive PSB2VP content used as MSTF-PSB10, MSTF-PSB20 and MSTF-PSB60. Magnification (on left of each row) and MSTF codes (on top of each column) are indicated. Approximate thickness of each film is indicated on the images D-F.

spherical features covering their surfaces. A representative AFM height image from a 1 × 1 μm^2 surface section of MSTF-PSB10 clearly displays this hierarchical structure featuring spherical assemblies (Fig. A10, Appendix A).

3.5. Ionic strength response of the ZCC and its effect on MSTF morphology

Polyzwitterions respond to changes in ionic strength, or rather the presence of small salt (Low Molecular weight Salt, LMS) ions through an interesting and unusual behavior termed the anti-polyelectrolyte effect [85,87,88]. In deionized water, polyzwitterions exhibit intra- and inter-molecular interactions between charged groups that form each zwitterion. This results in a relatively globular conformation. When a low molecular weight salt is added, its ions shield these interactions as each charged group comprising the zwitterionic molecule gets surrounded with its counter-ions and a hydration shell, leading to expansion of the polyzwitterion chain as well as zwitterionic groups themselves. Therefore, polyzwitterion chains are more expanded in saline solutions and behave in a more “hydrophilic” manner. This effect is likely to be further pronounced in ZCCs because the polyzwitterion side chains will not only change their degree of hydration but also their conformation.

In this framework, we can potentially utilize ionic strength as a tool to control and tune the self-assembly of ZCCs, and transport in the MSTFs using the external stimulus of changing water salinity. To test this hypothesis, we filtered NaCl solutions of increasing concentration through the MSTFs and measured the permeance, defined as the flux of the solution normalized by the applied pressure difference. The permeance decreased with increasing ionic strength (Fig. 8), in agreement

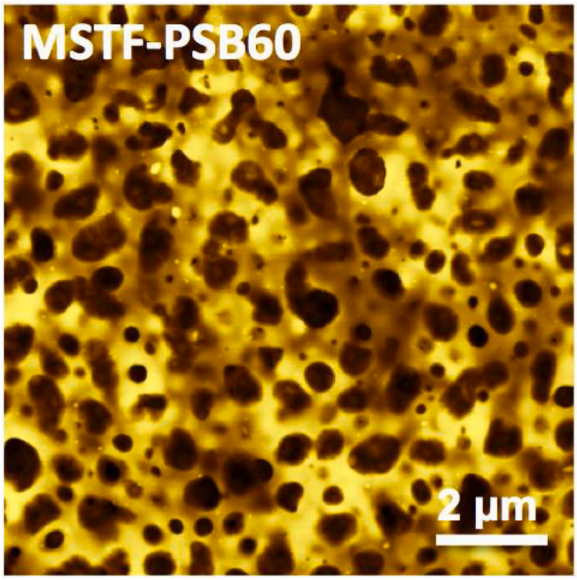

Fig. A9. AFM height image of MSTF-PSB60 from 10 × 10 µm^2 surface section with a z-range of 260 nm. The MSTF surface shows large pores with distorted morphology.

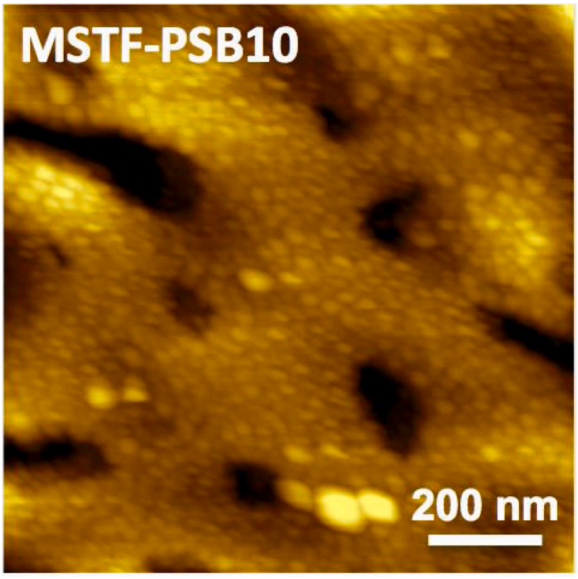

Fig. A10. AFM height image of MSTF-PSB10 from 1 × 1 µm^2 surface section with a z-range of 70 nm. Spherical micelles cover the film surface.

with previous reports involving zwitterionic membranes [112–114]. A potential explanation for the ionic strength responsive function is that, due to anti-polyelectrolyte effect [87], the zwitterionic side chains expand from the pore walls toward the center of the pores, leading to pore narrowing and decline in water flux. It is worth mentioning that neither flux decline nor pore narrowing observed at increased ionic strength reversed upon change to retrospective feed conditions. This hysteresis in chain swelling has previously been observed in other membranes that have a dense brush of responsive polymer chains lining their pores [115], which was attributed to hydrogen bonding and other intra- and interchain interactions. Similar effects are likely the cause of the irreversible changes in water flux observed in these ZCC membranes, though we believe it also warrants additional future study.

We expected this irreversible change in permeance to also be reflected in changes to membrane morphology. Furthermore, we expected to observe effects similar to that obtained with NaCl solutions using solutions commonly used in bioprocessing as well as routine fouling tests in the membrane field. For this purpose, we immersed a sample of MSTF-12s in phosphate buffered saline (PBS, 0.01 M, pH 7.4) solution overnight. We then rinsed it by immersing in deionized water and dried it. We imaged the film surface by AFM, and compared it with the surface of a sample that was not exposed to the saline solution. We observed a clear pore narrowing after the salt effect (Fig. 8A, B), further demonstrating a reduction in the effective pore size of the MSTF. This shows that the morphology and pore size of these membranes is sensitive not only to initial preparation conditions but also to exposure to salt after the film is solidified. This effect may have applications in tunable coatings and sensors.

4. Conclusions

We have developed porous thin films that form by the self-assembly of comb copolymers with zwitterionic side chains. In thin film formation, we systematically employed different preparation methods to apply our comb copolymers that feature various side chain length and density combinations. The self-assembled thin films showed various nanostructures including a partially connected network of short rod-like structures with an average diameter of 26 ± 5 nm or randomly interspersed spherical micelles ranging from 15 to 40 nm in diameter. We then studied the effect of the use of a porous substrate to create a mechanically supported thin film (MSTF) on self-assembled morphology. The use of a porous substrate led to distinct changes in surface morphology, leading to hierarchical features comprising 17 ± 5 nm spherical micelles together with larger pores 85 ± 45 nm in diameter. We could modify the size of these features by changing the air drying time or by using a zwitterionic homopolymer as an additive. Zwitterionic materials are also responsive to changes in salt concentration. To explore the effect of feed salinity on the permeance and morphology of the ZCC MSTFs, we performed filtration experiments using salt solutions with different concentrations. We observed that the water permeability and surface morphology exhibited irreversible changes upon exposure to water with high ionic strength. These results indicate ZCCs are versatile polymers that can lead to a wide variety of complex, nano-scale, hierarchical and tunable morphologies with various applications including water filtration and sensing.

Declaration of Competing Interest

A.A. owns a small equity in and serves as the Senior Scientific Advisor to ZwitterCo, Inc., which has licensed intellectual property related with this work from Tufts University.

Data availability

Data will be made available on request.

Acknowledgements

The authors gratefully acknowledge funding from the National Science Foundation (NSF) under Grants No. CBET-1553661 and DMR-2003629. The authors thank David Wilbur for help with NMR analysis, Prof. Peggy Cebe for access to the thermal analysis facilities, Prof. Qiaobing Xu for access to dynamic light scattering (DLS) and Atomic Force Microscopy (AFM) equipment, Prof. Samuel W. Thomas and Dr. Valentina Brega for access to and help with Gel Permeation Chromatography (GPC), and Grace Aro for experimental help with DLS measurements. FESEM imaging was conducted at Harvard University at the Center for Nanoscale Systems (CNS), a member of the National Nanotechnology Infrastructure Network (NNIN), supported by the National Science Foundation under NSF Award No. ECS-0335765. Transmission

Electron Microscopy (TEM) was conducted at the W.M. Keck foundation Biological Imaging Facility at the Whitehead Institute. Authors thank Nicki Watson at the Whitehead Institute for help with TEM image acquisition.

Supplementary materials

Supplementary material associated with this article can be found, in the online version, at doi:10.1016/j.apsadv.2022.100361.

Appendix A. Additional results and discussion

A1. Polymer synthesis and characterization

A1.1 Synthesis and characterization of backbone P(TFEMA-stat-CEM) copolymers

Two batches of backbone P(TFEMA-*stat*-CEM) were synthesized by Free Radical Polymerization (FRP) using different CEM frequency along the backbone, labeled PT30 and PT50, based on the approximate TFEMA:CEM molar ratios of 30:1 and 50:1, respectively. The composition of each copolymer was obtained using the integrated areas of the peaks a and e (Table S1) shown on the ^{1}H-NMR spectrum in Fig. S1. Each polymer was purified until there were no visible peaks associated with protons attached to vinyl groups of unreacted monomers, between 5.2-6.5 ppm.

The copolymer properties and reaction parameters for both batches are summarized in Table 1.

A1.2 Characterization of zwitterionic PTFEMA-g-SB2VP copolymers

To synthesize the comb copolymer PTFEMA-*g*-SB2VP, Activators ReGenerated by Electron Transfer ATRP (ARGET-ATRP) was conducted (Fig. S2A). Four batches of PTFEMA-*g*-SB2VP were synthesized by growing the SB2VP side chains at two different lengths from each of PT30 and PT50 backbone. The comb copolymers were encoded PT30-SB6, PT30-SB13, PT50-SB8 and PT50-SB12, with regard to the backbone used (PT30 or PT50) and the SB2VP side chain length. The ^{1}H-NMR spectrum of PT30-SB13 with peak assignments is shown in Fig. S2B.

All peaks with chemical shifts greater than 7 ppm were assigned to SB2VP units (h i j k), with four protons per SB2VP unit appearing in that region. The peak at 4.6 ppm was attributed to the convolution of CH_2 protons from TFEMA (a) and SB2VP (g). The integrated area under these peaks (Table A1), together with the TFEMA:Cl ratio from the composition of PTFEMA-*stat*-CEM used as the macroinitiator, were used to calculate the final comb copolymer composition. In addition, the P(TFEMA-*stat*-CEM) backbone peak at 3.8 ppm (e_1) shifts to 1.6 ppm (e_2) in PTFEMA-*g*-SB2VP, thus a residual peak at 3.8 ppm in the NMR spectrum of PTFEMA-*g*-SB2VP indicates unreacted Cl groups, and that can be used to estimate the initiation efficiency. With that, we obtained the percentage of chlorine atoms that initiated ARGET-ATRP (Table A2) from the ratio between the CEM peaks at 3.8 (e_1) and 4.2 ppm (d) (Fig. A2), attributed to the unreacted and total CEM contents, respectively.

Using the integrated peak areas and estimated initiation efficiencies listed in Table A2, we calculated the final comb copolymer composition and side-chain length as detailed below. First, we can write the two equations below using the ^{1}H-NMR peak areas:

$$Area_{h,\ i,j,k} = 4\ x\ n_{SB2VP}$$

$$Area_{a,\ g,l} = 2\ x\ n_{TFEMA} + 3\ x\ n_{SB2VP}$$

From these equations, we can obtain n_{SB2VP} and n_{TFEMA}, which are the relative number of moles of the SB2VP and TFEMA units in the copolymer. Using the backbone P(TFEMA-*stat*-CEM) composition (PTFEMA:CEM molar ratio of 30:1 and 50:1), we can also calculate the relative mole number for CEM units in the copolymer:

$$n_{CEM} = \frac{n_{TFEMA}}{30}\ or\ \frac{n_{TFEMA}}{50}$$

We can obtain the weight percentage of SB2VP in PTFEMA-*g*-SB2VP by using the relative mole number and molar mass of each component, where the molar mass of each component is $M_{w,\ TFEMA} = 168.11\ g/mol$, $M_{w,\ CEM} = 148.59\ g/mol$ and $M_{w,\ SB2VP} = 227.28\ g/mol$. The weight percentage of SB2VP (w_{SB2VP}) can be obtained as:

$$w_{SB2VP} = \frac{n_{SB2VP}\ x\ M_{w,\ SB2VP}}{\left(n_{SB2VP}\ x\ M_{w,\ SB2VP}\right) + \left(n_{TFEMA}\ x\ M_{w,\ TFEMA}\right) + \left(n_{CEM}\ x\ M_{w,\ CEM}\right)}\ x\ 100$$

To obtain the average side-chain length, we need to calculate the number of Cl units that have been initiated ($n_{CEM,\ initiated}$) during ARGET-ATRP using the initiation efficiency (i):

$$n_{CEM,initiated} = n_{CEM}\ x\ i$$

Then, we can estimate the average side-chain length ($n_{side-chain}$), which is simply the average number of SB2VP units propagated from each activated Cl, calculated as:

$$n_{side-chain} = \frac{n_{SB2VP}}{n_{CEM,initiated}}$$

The mass composition and side-chain length of each comb copolymer are listed in Table 2.

A2. Thermal transitions of PT50-based copolymers by differential scanning calorimetry

Fig. A3 shows the Differential Scanning Calorimetry (DSC) thermograms from reversible heat flow versus temperature plot for comb copolymers derived from the PT50 backbone. All the PT50-based copolymers display a glass transition temperature (T_g) at around 80 °C, and this T_g does not shift from the backbone to comb copolymers, indicative of phase separation.

A3. Thin film preparation and characterization

A3.1. Thin films deposited on glass substrate by spin coating without hydration

We applied the 3 wt.% comb copolymer solution in trifluoroethanol (TFE) as a thin film on glass substrate following three different procedures: (1) spin coating; (2) spin coating followed by immersion in deionized water (hydration); and (3) casting followed by air drying for 12 s, non-solvent induced phase separation (NIPS) in isopropanol bath and immersion in deionized water. Atomic Force Microscopy (AFM) images in Fig. A4 show that the thin films are nearly featureless when prepared by spin coating only to create a fairly smooth film.

A3.2. Thin films deposited on transmission electron microscopy (TEM) grid using different solvent evaporation times prior to non-solvent induced phase separation (NIPS)

To study the self-assembly of PT30-SB13 copolymer during NIPS procedure, we simulated the thin film formation by NIPS on TEM grids. First, a 0.1 wt.% copolymer solution in trifluoroethanol (TFE) was drop-cast on the grid. The solvent was allowed to air dry for a predetermined period of time, followed by isopropanol immersion for 10 min, and then water immersion for 10 min. Films were prepared with varying drying times as 5 s, 12 s, or 25 s because self-assembly of amphiphilic copolymers in solution may evolve with the progression of solvent evaporation. For comparison, one film was prepared by air-drying only without any immersion step. Fig. A5 shows that NIPS procedure leads to formation of a continuous tubular network, whereas air-drying yields randomly distributed, isolated assemblies. On the other hand, we did not observe an evident change in film morphology by varying the drying time to 5 or 25 s prior to NIPS.

A4. Preparation and characterization of mechanically supported thin film (MSTF) with selective layer on a porous support

A4.1. Support membrane cross-sectional and surface morphology

Fig. A6 shows the cross-sectional FESEM and surface AFM images of the commercial PVDF400R ultrafiltration membrane used as support in the MSTFs. To form the MSTF, a thin layer of the PT30-SB13 copolymer was applied as a selective layer on the PVDF400R support.

A4.2. Mechanically supported thin film (MSTF) prepared using different solvent evaporation times prior to non-solvent induced phase separation (NIPS)

In MSTF preparation, we cast the 3 wt.% PT30-SB13 solution in trifluoroethanol (TFE) on PVDF400R support, air-dried for a predetermined period of time to allow solvent evaporation, and then immersed the MSTF into an isopropanol bath for one hour to precipitate out the copolymer. Air-drying time was employed as 5, 12 or 25 s, and the corresponding MSTFs were encoded MSTF-5s, MSTF-12s, and MSTF-25s, accordingly. Finally, the MSTF was immersed and stored in a water bath. Fig. A7A-C shows that surfaces of all the MSTFs feature a macroporous structure with pores ~30-200 nm in diameter spread randomly across the surface.

Pore diameter and pore depth estimated from AFM image of each MSTF were 85 ± 30 and 16 ± 6 nm for MSTF-5s, 85 ± 45 and 20 ± 10 nm for MSTF-12s, and 140 ± 50 and 25 ± 9 nm for MSTF-25s. (Fig. A7)

A4.3. Mechanically supported thin film (MSTF) prepared using zwitterionic homopolymer additive

To modify the pore size and morphology of MSTF-12s, we added different ratios of homopolymer poly sulfobetaine-2-vinyl pyridine (PSB2VP) into the PT30-SB13 copolymer solution in TFE, and then followed the film formation procedure identical to that of MSTF-12s; 12 s air-drying preceding NIPS in isopropanol and water immersion. Additive PSB2VP content was fixed at 10, 20 or 60 wt.% of the copolymer PT30-SB13, where the PT30-SB13 composition was set to be 3 wt.% of the casting solution. Resulting MSTFs were encoded MSTF-PSB10, MSTF-PSB20 and MSTF-PSB60, correspondingly. Cross-sectional FESEM images in Fig. A8 show that selective layer structure is similar for all the MSTFs, dense with a thickness in 120-170 nm range.

As seen in Fig. A9, addition of 60 wt.% PSB2VP with respect to copolymer PT30-SB13 (MSTF-PSB60) led to large pores with distorted morphology. Fig. A10 shows that spherical micelles are ubiquitous on the film surface.

References

[1] C.N. Walker, K.C. Bryson, R.C. Hayward, G.N. Tew, Wide bicontinuous compositional windows from co-networks made with telechelic macromonomers, ACS Nano 8 (2014) 12376–12385.

[2] K.G. Yager, E. Lai, C.T. Black, Self-assembled phases of block copolymer blend thin films, ACS Nano 8 (2014) 10582–10588.

[3] S.W. Hong, W. Gu, J. Huh, B.R. Sveinbjornsson, G. Jeong, R.H. Grubbs, T. P. Russell, On the self-assembly of brush block copolymers in thin films, ACS Nano 7 (2013) 9684–9692.

[4] H. Tran, K. Ronaldson, N.A. Bailey, N.A. Lynd, K.L. Killops, G. Vunjak-Novakovic, L.M. Campos, Hierarchically ordered nanopatterns for spatial control of biomolecules, ACS Nano 8 (2014) 11846–11853.

[5] R.M. Dorin, H. Sai, U. Wiesner, Hierarchically Porous Materials from Block Copolymers, Chem. Mater. 26 (2014) 339–347.

[6] A. Muñoz-Bonilla, E. Ibarboure, E. Papon, J. Rodriguez-Hernandez, Self-organized hierarchical structures in polymer surfaces: self-assembled nanostructures within breath figures, Langmuir 25 (2009) 6493–6499.

[7] P. Kaner, P. Bengani-Lutz, I. Sadeghi, A. Asatekin, Responsive filtration membranes by polymer self-assembly, Technology 4 (2016) 1–12.

[8] W.A. Phillip, B. O'Neill, M. Rodwogin, M.A. Hillmyer, E. Cussler, Self-assembled block copolymer thin films as water filtration membranes, ACS Appl. Mater. Interfaces 2 (2010) 847–853.

[9] I. Sadeghi, J. Kronenberg, A. Asatekin, Selective transport through membranes with charged nanochannels formed by scalable self-assembly of random copolymer micelles, ACS Nano 12 (2018) 95–108.

[10] I. Sadeghi, A. Asatekin, Spontaneous self-assembly and micellization of random copolymers in organic solvents, Macromol. Chem. Phys. 218 (2017), 1700226.

[11] P. Bengani-Lutz, I. Sadeghi, S.J. Lounder, M.J. Panzer, A. Asatekin, High flux membranes with ultrathin zwitterionic copolymer selective layers with ~1 nm pores using an ionic liquid cosolvent, ACS Appl. Polym. Mater. 1 (2019) 1954–1959.

[12] X. Feng, M.E. Tousley, M.G. Cowan, B.R. Wiesenauer, S. Nejati, Y. Choo, R. D. Noble, M. Elimelech, D.L. Gin, C.O. Osuji, Scalable fabrication of polymer membranes with vertically aligned 1 nm pores by magnetic field directed self-assembly, ACS Nano 8 (2014) 11977–11986.

[13] A. Akthakul, R.F. Salinaro, A.M. Mayes, Antifouling polymer membranes with subnanometer size selectivity, Macromolecules 37 (2004) 7663–7668.

[14] P. Bengani, Y. Kou, A. Asatekin, Zwitterionic copolymer self-assembly for fouling resistant, high flux membranes with size-based small molecule selectivity, J. Membr. Sci. 493 (2015) 755–765.

[15] P. Bengani-Lutz, E. Converse, P. Cebe, A. Asatekin, Self-assembling zwitterionic copolymers as membrane selective layers with excellent fouling resistance: effect of zwitterion chemistry, ACS Appl. Mater. Interfaces 9 (2017) 20859–20872.

[16] P. Kaner, X. Hu, S.W. Thomas, A. Asatekin, Self-cleaning membranes from comb-shaped copolymers with photoresponsive side groups, ACS Appl. Mater. Interfaces 9 (2017) 13619–13631.

[17] P. Kaner, E. Rubakh, D.H. Kim, A. Asatekin, Zwitterion-containing polymer additives for fouling resistant ultrafiltration membranes, J. Membr. Sci. 533 (2017) 141–159.

[18] S.J. Lounder, A. Asatekin, Zwitterionic Ion-Selective membranes with tunable subnanometer pores and excellent fouling resistance, Chem. Mater. 33 (2021) 4408–4416.

[19] S.J. Lounder, A. Asatekin, Fouling- and chlorine-resistant nanofiltration membranes fabricated from charged zwitterionic amphiphilic copolymers, ACS Appl. Polym. Mater. 4 (2022) 7998–8008.
[20] C. Park, J. Yoon, E.L. Thomas, Enabling nanotechnology with self assembled block copolymer patterns, Polymer 44 (2003) 6725–6760.
[21] R.A. Segalman, Patterning with block copolymer thin films, Mater. Sci. Eng. R. 48 (2005) 191–226.
[22] O. Ikkala, G. ten Brinke, Functional materials based on self-assembly of polymeric supramolecules, Science 295 (2002) 2407–2409.
[23] S.O. Kim, H.H. Solak, M.P. Stoykovich, N.J. Ferrier, J.J. de Pablo, P.F. Nealey, Epitaxial self-assembly of block copolymers on lithographically defined nanopatterned substrates, Nature 424 (2003) 411.
[24] J.K. Cox, A. Eisenberg, R.B. Lennox, Patterned surfaces via self-assembly, Curr. Opin. Colloid Interface Sci. 4 (1999) 52–59.
[25] G. Krausch, R. Magerle, Nanostructured thin films via self-assembly of block copolymers, Adv. Mater. 14 (2002) 1579–1583.
[26] J.N. Albert, T.H. Epps III, Self-assembly of block copolymer thin films, Mater. Today 13 (2010) 24–33.
[27] Y. Lin, A. Böker, J. He, K. Sill, H. Xiang, C. Abetz, X. Li, J. Wang, T. Emrick, S. Long, Self-directed self-assembly of nanoparticle/copolymer mixtures, Nature 434 (2005) 55.
[28] L. Wang, J. Lin, X. Zhang, Hierarchical microstructures self-assembled from polymer systems, Polymer 54 (2013) 3427–3442.
[29] K. Koch, W. Barthlott, Superhydrophobic and superhydrophilic plant surfaces: an inspiration for biomimetic materials, Philos. Trans. R. Soc. A 367 (2009) 1487–1509.
[30] K. Koch, B. Bhushan, Y.C. Jung, W. Barthlott, Fabrication of artificial lotus leaves and significance of hierarchical structure for superhydrophobicity and low adhesion, Soft Matter 5 (2009) 1386–1393.
[31] B. Bhushan, Y.C. Jung, K. Koch, Micro-, nano- and hierarchical structures for superhydrophobicity, self-cleaning and low adhesion, Philos. Trans. R. Soc. A 367 (2009) 1631–1672.
[32] H. Yao, H. Gao, Mechanics of robust and releasable adhesion in biology: bottom–up designed hierarchical structures of gecko, J. Mech. Phys. Solids 54 (2006) 1120–1146.
[33] H. Gao, X. Wang, H. Yao, S. Gorb, E. Arzt, Mechanics of hierarchical adhesion structures of geckos, Mech. Mater. 37 (2005) 275–285.
[34] P. Fratzl, Biomimetic materials research: what can we really learn from nature's structural materials? J. R. Soc. Interface 4 (2007) 637–642.
[35] C. Sanchez, H. Arribart, M.M.G. Guille, Biomimetism and bioinspiration as tools for the design of innovative materials and systems, Nat. Mater. 4 (2005) 277.
[36] P. Kwong, S. Seidel, M. Gupta, Solventless fabrication of porous-on-porous materials, ACS Appl. Mater. Interfaces 5 (2013) 9714–9718.
[37] M. Shimomura, T. Sawadaishi, Bottom-up strategy of materials fabrication: a new trend in nanotechnology of soft materials, Curr. Opin. Colloid Interface Sci. 6 (2001) 11–16.
[38] S.P. Nunes, A. Car, From charge-mosaic to micelle self-assembly: block copolymer membranes in the last 40 years, Ind. Eng. Chem. 52 (2012) 993–1003.
[39] F.H. Schacher, P.A. Rupar, I. Manners, Functional block copolymers: nanostructured materials with emerging applications, Angew. Chem. Int. Ed. 51 (2012) 7898–7921.
[40] Y. Mai, A. Eisenberg, Self-assembly of block copolymers, Chem. Soc. Rev. 41 (2012) 5969–5985.
[41] Y. Matsushita, A. Takano, K. Hayashida, T. Asari, A. Noro, Hierarchical nanophase-separated structures created by precisely-designed polymers with complexity, Polymer 50 (2009) 2191–2203.
[42] O. Ikkala, G. ten Brinke, Hierarchical self-assembly in polymeric complexes: towards functional materials, Chem. Commun. (2004) 2131–2137. https://pubs.rsc.org/en/content/articlelanding/2004/cc/b403983a.
[43] V. Abetz, Isoporous block copolymer membranes, Macromol. Rapid Commun. 36 (2015) 10–22.
[44] H. Qiu, Y. Gao, C.E. Boott, O.E.C. Gould, R.L. Harniman, M.J. Miles, S.E.D. Webb, M.A. Winnik, I. Manners, Uniform patchy and hollow rectangular platelet micelles from crystallizable polymer blends, Science 352 (2016) 697–701.
[45] A.H. Gröschel, A.H.E. Müller, Self-assembly concepts for multicompartment nanostructures, Nanoscale 7 (2015) 11841–11876.
[46] C.M. Bates, M.J. Maher, D.W. Janes, C.J. Ellison, C.G. Willson, Block copolymer lithography, Macromolecules 47 (2014) 2–12.
[47] S. Darling, Directing the self-assembly of block copolymers, Prog. Polym. Sci. 32 (2007) 1152–1204.
[48] L. Pavesi, E.V. Buzaneva, Frontiers of Nano-Optoelectronic Systems, Kluwer Academic Publishers, Dordrecht; Boston, 2000.
[49] G. Hattori, M. Takenaka, M. Sawamoto, T. Terashima, Nanostructured materials via the pendant self-assembly of amphiphilic crystalline random copolymers, J. Am. Chem. Soc. 140 (2018) 8376–8379.
[50] L. Li, K. Raghupathi, C. Song, P. Prasad, S. Thayumanavan, Self-assembly of random copolymers, Chem. Commun. 50 (2014) 13417–13432.
[51] N. Badi, D. Chan-Seng, J.F. Lutz, Microstructure control: an underestimated parameter in recent polymer design, Macromol. Chem. Phys. 214 (2013) 135–142.
[52] M.P. Dugas, G. Van Every, B. Park, J.R. Hoffman, R.J. LaRue, A.M. Bush, Y. Zhang, J.L. Schaefer, D.R. Latulippe, W.A. Phillip, Resilient hollow fiber nanofiltration membranes fabricated from crosslinkable phase-separated copolymers, Mol. Syst. Des. Eng. 5 (2020) 943–953.
[53] X. He, M.-S. Hsiao, Charlotte E. Boott, Robert L. Harniman, A. Nazemi, X. Li, A Mitchell, Two-dimensional assemblies from crystallizable homopolymers with charged termini, Nat. Mater. 16 (2017) 481–488.
[54] S. Qu, T. Dilenschneider, W.A. Phillip, Preparation of chemically-tailored copolymer membranes with tunable ion transport properties, ACS. Appl. Mater. Interfaces 7 (2015) 19746–19754.
[55] A. Asatekin, A.M. Mayes, Responsive pore size properties of composite NF membranes based on PVDF graft copolymers, Sep. Sci. Technol. 44 (2009) 3330–3345.
[56] A. Asatekin, E.A. Olivetti, A.M. Mayes, Fouling resistant, high flux nanofiltration membranes from polyacrylonitrile-graft-poly(ethylene oxide), J. Membr. Sci. 332 (2009) 6–12. XXX.
[57] R. Verduzco, X. Li, S.L. Pesek, G.E. Stein, Structure, function, self-assembly, and applications of bottlebrush copolymers, Chem. Soc. Rev. 44 (2015) 2405–2420.
[58] J. Bolton, T.S. Bailey, J. Rzayev, Large pore size nanoporous materials from the self-assembly of asymmetric bottlebrush block copolymers, Nano Lett. 11 (2011) 998–1001.
[59] A. Hanisch, A.H. Gröschel, M. Förtsch, T.I. Löbling, F.H. Schacher, A.H.E. Müller, Hierarchical self-assembly of miktoarm star polymers containing a polycationic segment: a general concept, Polymer 54 (2013) 4528–4537.
[60] K. Khanna, S. Varshney, A. Kakkar, Miktoarm star polymers: advances in synthesis, self-assembly, and applications, Polym. Chem. 1 (2010) 1171–1185.
[61] K. Matyjaszewski, N.V. Tsarevsky, Nanostructured functional materials prepared by atom transfer radical polymerization, Nat. Chem. 1 (2009) 276–288.
[62] M.B. Runge, N.B. Bowden, Synthesis of high molecular weight comb block copolymers and their assembly into ordered morphologies in the solid state, J. Am. Chem. Soc. 129 (2007) 10551–10560.
[63] J. Bolton, T.S. Bailey, J. Rzayev, Large pore size nanoporous materials from the self-assembly of asymmetric bottlebrush block copolymers, Nano Lett. 11 (2011) 998–1001.
[64] R. Stepanyan, A. Subbotin, G. Ten Brinke, Comb copolymer brush with chemically different side chains, Macromolecules 35 (2002) 5640–5648.
[65] O. Borisov, E. Zhulina, Amphiphilic graft copolymer in a selective solvent: intramolecular structures and conformational transitions, Macromolecules 38 (2005) 2506–2514.
[66] P. Košovan, J. Kuldová, Z. Limpouchová, K. Procházka, E.B. Zhulina, O. V. Borisov, Amphiphilic graft copolymers in selective solvents: molecular dynamics simulations and scaling theory, Macromolecules 42 (2009) 6748–6760.
[67] E.Y. Kramarenko, O. Pevnaya, A. Khokhlov, Stoichiometric polyelectrolyte complexes as comb copolymers, J. Chem. Phys. 122 (2005), 084902.
[68] H.-Y. Chang, Y.-L. Lin, Y.-J. Sheng, H.-K. Tsao, Structural characteristics and fusion pathways of onion-like multilayered polymersome formed by amphiphilic comb-like graft copolymers, Macromolecules 46 (2013) 5644–5656.
[69] X. Lian, D. Wu, X. Song, H. Zhao, Synthesis and self-assembly of amphiphilic asymmetric macromolecular brushes, Macromolecules 43 (2010) 7434–7445.
[70] M. Li, G.L. Li, Z. Zhang, J. Li, K.-G. Neoh, E.-T. Kang, Self-assembly of pH-responsive and fluorescent comb-like amphiphilic copolymers in aqueous media, Polymer 51 (2010) 3377–3386.
[71] H. Wang, Y.-T. Liu, H.-J. Qian, Z.-Y. Lu, Dissipative particle dynamics simulation study on complex structure transitions of vesicles formed by comb-like block copolymers, Polymer 52 (2011) 2094–2101.
[72] C. Zheng, L. Qiu, K. Zhu, Novel polymersomes based on amphiphilic graft polyphosphazenes and their encapsulation of water-soluble anti-cancer drug, Polymer 50 (2009) 1173–1177.
[73] X. Li, J. Ji, X. Wang, Y. Wang, J. Shen, Stability and drug loading of spontaneous vesicles of comb-Like PEG derivates, Macromol. Rapid Commun. 28 (2007) 660–665.
[74] M. Ehrmann, R. Muller, J.C. Galin, C.G. Bazuin, Statistical n-butyl acrylate-(sulfopropyl) ammonium betaine copolymers. 4. dynamic mechanical properties, Macromolecules 26 (1993) 4910–4918.
[75] M. Ehrmann, A. Mathis, B. Meurer, M. Scheer, J.C. Galin, Statistical n-butyl acrylate-(sulfopropyl) ammonium betaine copolymers. 2. structural studies, Macromolecules 25 (1992) 2253–2261.
[76] M. Ehrmann, R. Muller, J.C. Galin, C.G. Bazuin, Statistical N-butyl acrylate-(sulfopropyl) ammonium betaine copolymers. 4, Dyn. Mech. Prop. Macromol. 26 (1993) 4910–4918.
[77] M. Ehrmann, A. Mathis, B. Meurer, M. Scheer, J.C. Galin, Statistical N-butyl acrylate-(sulfopropyl) ammonium betaine copolymers. 2, Struct. Stud. Macromol. 25 (1992) 2253–2261.
[78] M.G. Ehrmann, J.C. Meurer, Statistical n-butyl acrylate-sulfopropyl betaine copolymers. 3. Domain size determination by solid-state NMR spectroscopy, Macromolecules 26 (1993) 988–993.
[79] A. Mathis, Y.L. Zheng, J.C. Galin, Random ethylacrylate zwitterionic copolymers: 3. Microphase separation as a function of the zwitterion structure, Polymer 32 (1991) 3080–3085.
[80] Y.L. Zheng, M. Galin, J.C. Galin, Random ethylacrylate-sulphonatopropylbetaine copolymers. 1. Synthesis and characterization, Polymer 29 (1988) 724–730.
[81] T.Y. Wu, F.L. Beyer, R.H. Brown, R.B. Moore, T.E. Long, Influence of zwitterions on thermomechanical properties and morphology of acrylic copolymers: implications for electroactive applications, Macromolecules 44 (2011) 8056–8063.
[82] A.B. Lowe, N.C. Billingham, S.P. Armes, Synthesis and properties of low-polydispersity poly(sulfopropylbetaine)s and their block copolymers, Macromolecules 32 (1999) 2141–2148.

[83] Z. Tuzar, H. Pospisil, J. Plestil, A.B. Lowe, F.L. Baines, N.C. Billingham, S. P. Armes, Micelles of hydrophilic-hydrophobic poly(sulfobetaine)-based block copolymers, Macromolecules 30 (1997) 2509–2512.
[84] D. Wang, T. Wu, X. Wan, X. Wang, S. Liu, Purely salt-responsive micelle formation and inversion based on a novel schizophrenic sulfobetaine block copolymer: structure and kinetics of micellization, Langmuir 23 (2007) 11866–11874.
[85] J. Bredas, R. Chance, R. Silbey, Head-head interactions in zwitterionic associating polymers, Macromolecules 21 (1988) 1633–1639.
[86] Y. Chen, Y. Zhang, Y. Wang, C. Sun, C. Zhang, Synthesis, characterization, and self-assembly of amphiphilic fluorinated gradient copolymer, J. Appl. Polym. Sci. 127 (2013) 1485–1492.
[87] G.S. Georgiev, E.B. Kamenska, E.D. Vassileva, I.P. Kamenova, V.T. Georgieva, S. B. Iliev, I.A. Ivanov, Self-assembly, antipolyelectrolyte effect, and nonbiofouling properties of polyzwitterions, Biomacromolecules 7 (2006) 1329–1334.
[88] O. Azzaroni, A.A. Brown, W.T.S. Huck, UCST wetting transitions of polyzwitterionic brushes driven by self-association, Angew. Chem. Int. Ed. 118 (2006) 1802–1806.
[89] M. Galin, A. Chapoton, J.-C. Galin, Dielectric increments, intercharge distances and conformation of quaternary ammonioalkylsulfonates and alkoxydicyanoethenolates in aqueous and trifluoroethanol solutions, J. Chem. Soc. Perkin Trans. 2 (1993) 545–553.
[90] J.S. Wang, K. Matyjaszewski, Controlled/“ living” radical polymerization. Halogen atom transfer radical polymerization promoted by a Cu (I)/Cu (II) redox process, Macromolecules 28 (1995) 7901–7910.
[91] A.P. Purdy, O. Kuyinu, Synthesis and dielectric properties of some zwitterionic polymers, Polymer Preprints 50 (2009) 677–678.
[92] R.J. Young, P.A. Lovell. Introduction to Polymers, CRC press, Boca Raton , FL, USA, 2011.
[93] C.A. Schneider, W.S. Rasband, K.W. Eliceiri, NIH Image to ImageJ: 25 years of image analysis, Nat. Methods 9 (2012) 671–675.
[94] M. Galin, E. Marchal, A. Mathis, B. Meurer, Y.M. Soto, J. Galin, Poly (sulphopropylbetaines): 3. bulk properties, Polym. 28 (1987) 1937–1944.
[95] J.S. Wang, K. Matyjaszewski, Controlled/" living" radical polymerization. halogen atom transfer radical polymerization promoted by a Cu (I)/Cu (II) redox process, Macromolecules 28 (1995) 7901–7910.
[96] R.J. Young, P.A. Lovell, Introduction to Polymers, CRC press, Boca Raton, FL, USA, 2011.
[97] J. Rodriguez-Hernandez, F. Chécot, Y. Gnanou, S. Lecommandoux, Toward ‘smart’nano-objects by self-assembly of block copolymers in solution, Prog. Polym. Sci. 30 (2005) 691–724.
[98] M. Galin, E. Marchal, A. Mathis, B. Meurer, Y.M. Soto, J. Galin, Poly (sulphopropylbetaines): 3. Bulk properties, Polymer 28 (1987) 1937–1944.
[99] A. Clark, Y. Biswas, M.E. Taylor, A. Asatekin, M.J. Panzer, C. Schick, P. Cebe, Glass-forming ability of polyzwitterions, Macromolecules 54 (2021) 10126–10134.
[100] S. Kurata, N. Yamazaki, Mechanical properties of poly(alkyl a-fluoroacrylate) s as denture-base materials, J. Dent. Res. 68 (1989) 481–483.
[101] O. Ratcharak, A. Sane, Surface coating with poly(trifluoroethyl methacrylate) through rapid expansion of supercritical CO_2 solutions, J. Supercrit. Fluids 89 (2014) 106–112.
[102] B.S. Lalia, V. Kochkodan, R. Hashaikeh, N. Hilal, A review on membrane fabrication: structure, properties and performance relationship, Desalination 326 (2013) 77–95.
[103] K.W. Tan, B. Jung, J.G. Werner, E.R. Rhoades, M.O. Thompson, U. Wiesner, Transient laser heating induced hierarchical porous structures from block copolymer–directed self-assembly, Science 349 (2015) 54–58.
[104] N.A. Ochoa, P. Prádanos, L. Palacio, C. Pagliero, J. Marchese, A. Hernández, Pore size distributions based on AFM imaging and retention of multidisperse polymer solutes: characterisation of polyethersulfone UF membranes with dopes containing different PVP, J. Membr. Sci. 187 (2001) 227–237.
[105] C.G. Gamys, A. Vlad, O. Bertrand, J.-F. Gohy, Functionalized nanoporous thin films from blends of block copolymers and homopolymers interacting via hydrogen bonding, Macromol. Chem. Phys. 213 (2012) 2075–2080.
[106] S.Y. Yang, I. Ryu, H.Y. Kim, J.K. Kim, S.K. Jang, T.P. Russell, Nanoporous membranes with ultrahigh selectivity and flux for the filtration of viruses, Adv. Mater. 18 (2006) 709–712.
[107] U.Y. Jeong, D.Y. Ryu, J.K. Kim, D.H. Kim, X.D. Wu, T.P. Russell, Precise control of nanopore size in thin film using mixtures of asymmetric block copolymer and homopolymer, Macromolecules 36 (2003) 10126–10129.
[108] J.I. Clodt, S. Rangou, A. Schroder, K. Buhr, J. Hahn, A. Jung, V. Filiz, V. Abetz, Carbohydrates as additives for the formation of isoporous PS-b-P4VP Diblock copolymer membranes, Macromol. Rapid Commun. 34 (2013) 190–194.
[109] C.-y. Yang, G.-d. Zhu, Z. Yi, Y. Zhou, C.-j. Gao, Critical contributions of additives on the fabrication of asymmetric isoporous membranes from block copolymers: a review, Chem Eng J 424 (2021), 128912.
[110] S.P. Nunes, R. Sougrat, B. Hooghan, D.H. Anjum, A.R. Behzad, L. Zhao, N. Pradeep, I. Pinnau, U. Vainio, K.V. Peinemann, Ultraporous films with uniform nanochannels by block copolymer micelles assembly, Macromolecules 43 (2010) 8079–8085.
[111] W.A. Phillip, R.M. Dorin, J. Werner, E.M.V. Hoek, U. Wiesner, M. Elimelech, Tuning structure and properties of graded triblock terpolymer-based mesoporous and hybrid films, Nano Lett. 11 (2011) 2892–2900.
[112] G. Zhai, S.C. Toh, W.L. Tan, E.T. Kang, K.G. Neoh, C.C. Huang, D.J. Liaw, Poly (vinylidene fluoride) with grafted zwitterionic polymer side chains for electrolyte-responsive microfiltration membranes, Langmuir 19 (2003) 7030–7037.
[113] Y.-H. Zhao, K.-H. Wee, R. Bai, A novel electrolyte-responsive membrane with tunable permeation selectivity for protein purification, ACS Appl. Mater. Interfaces 2 (2009) 203–211.
[114] S.J. Lounder, P.T. Wright, L. Mazzaferro, A. Asatekin, Fouling-resistant membranes with tunable pore size fabricated using cross-linkable copolymers with high zwitterion content, J. Membr. Sci. Lett. 2 (2022), 100019.
[115] J.L. Weidman, R.A. Mulvenna, B.W. Boudouris, W.A. Phillip, Unusually stable hysteresis in the ph-response of poly(acrylic acid) brushes confined within nanoporous block polymer thin films, J. Am. Chem. Soc. 138 (2016) 7030–7039.